NASA CR-144503
ERIM 101700-27-F

Final Report

MACHINE PROCESSING OF S-192 AND SUPPORTING AIRCRAFT DATA - STUDIES OF ATMOSPHERIC EFFECTS, AGRICULTURAL CLASSIFICATIONS, AND LAND RESOURCE MAPPING

F. THOMSON
Infrared and Optics Division

AUGUST 1975

Prepared for
NATIONAL AERONAUTICS AND SPACE ADMINISTRATION

Johnson Space Center
Houston, Texas 77058
Contract No. NAS9-13272

ENVIRONMENTAL
RESEARCH INSTITUTE OF MICHIGAN
FORMERLY WILLOW RUN LABORATORIES, THE UNIVERSITY OF MICHIGAN
BOX 618 • ANN ARBOR • MICHIGAN 48107

TECHNICAL REPORT STANDARD TITLE PAGE

1. Report No.	2. Government Accession No.	3. Recipient's Catalog No.
NASA CR-ERIM 101700-27-F		

4. Title and Subtitle	5. Report Date
MACHINE PROCESSING OF S-192 AND SUPPORTING DATA — STUDIES OF ATMOSPHERIC EFFECTS, AGRICULTURAL CLASSIFICATION, AND LAND RESOURCE MAPPING	August 1975
	6. Performing Organization Code
7. Author(s)	8. Performing Organization Report No.
F. Thomson	101700-27-F
9. Performing Organization Name and Address	10. Work Unit No.
Environmental Research Institute of Michigan Infrared and Optics Division P.O. Box 618 Ann Arbor, Michigan 48107 (313) 994-1200	11. Contract or Grant No. NAS9-13272
	13. Type of Report and Period Covered
12. Sponsoring Agency Name and Address	Final Report 8 March 1973 through 30 August 1975
National Aeronautics and Space Administration Johnson Space Center Houston, Texas 77058	14. Sponsoring Agency Code

15. Supplementary Notes

Mr. Larry B. York (Code TF6) was technical monitor.

16. Abstract

Work is reported on two tasks of machine processing of S-192 Multispectral scanner data. In the first task, the effects of changing atmospheric and base altitude on the ability to machine-classify agricultural crops were investigated. A classifier and atmospheric effects simulation model was devised and its accuracy verified by comparison of its predicted results with S-192 processed results.

In the second task, land resource maps of a mountainous area near Cripple Creek, Colorado were prepared from S-192 data collected on 4 August 1973. The work was a cooperative effort between ERIM and Dr. Harry Smedes of USGS-Denver.

17. Key Words	18. Distribution Statement
Atmospheric Effects Pattern Recognition Multispectral Scanner Skylab Earth Resources Experiment	Initial distribution is listed at the end of this document.

19. Security Classif. (of this report)	20. Security Classif. (of this page)	21. No. of Pages	22. Price
Unclassified	Unclassified	92	

PREFACE

Work is reported covering an investigation of atmospheric effects on pattern classifier or pattern recognition performance, and land resource mapping. S-192 Skylab multispectral scanner and supporting aircraft data were examined from 8 March 1973 - 30 August 1975.

The work was performed in the Infrared and Optics Division of the Environmental Research Institute of Michigan under the direction of Richard R. Legault. The principal investigator was Frederick J. Thomson. Significant technical contributions were made by David Zuk, Frank Carioti and Janice Tone (field work); Frank Sadowski, Tom Austin, Daniel Rice and Harvey Wagner (computer processing); and Dr. Harry Smedes (USGS) and Jon Ranson (Colorado State University) (Cripple Creek Study).

CONTENTS

FIGURES

TABLES

MACHINE PROCESSING OF S-192 AND SUPPORTING AIRCRAFT DATA — STUDIES OF ATMOSPHERIC EFFECTS, AGRICULTURAL CLASSIFICATION, AND LAND RESOURCE MAPPING

1

INTRODUCTION

This is the final report on contract NAS9-13272 dealing with a study of changes in pattern recognition performance caused by variations in atmospheric state over the area of interest. As a secondary goal, we assessed the utility of S-192 data for mapping terrain types in the Cripple Creek, Colorado area. The work was conducted in the Infrared and Optics Division by Frank Sadowski and Thomas Austin, under the direction of Fred Thomson. The NASA technical monitor was Larry B. York.

1.1 STATEMENT OF THE PROBLEM

To be cost-effective, earth resources surveys using satellite or aircraft multispectral data must be done over large areas. If pattern recognition techniques are used as an information extraction tool to provide the user the information he wants from the multispectral data, those techniques too must be effective over large areas.

The use of pattern recognition techniques involves the assumption that the spectral radiance signatures of objects or classes to be recognized are sufficiently unique that these classes can be separated by the pattern classifier or recognizer. Further, training sets are required, either to teach the recognizer what the classes to be recognized look like or to evaluate which spectral clusters correspond to which objects to be recognized. Because time taken to train the recognizer cannot be spent processing data, we would prefer to train as infrequently as possible.

In operations, we must retrain whenever the conditions of objects change materially (e.g., vegetation phenologic state) or when the

conditions of measurement change (e.g. solar illumination, atmospheric state, or sensor performance). Preprocessing techniques can partially compensate for changes in measurement conditions and allow an extension of the area over which a given set of training set signatures will yield good results.

But utilization of preprocessing techniques may also slow the processing of data, especially when parameters for the preprocessing algorithms must be estimated from the data. Hence the question arises — How often, or under what conditions does pattern recognition performance suffer so much that preprocessing must be performed (or existing preprocessing altered) to retain good accuracy? That is the question addressed by the first phase of this work.

The second phase of this work addresses the utility of S-192 to map terrain features in the Cripple Creek, Colorado area. The ability to map these terrain features accurately and periodically is of value to Federal, State, and Regional resource managers in their management of the area. Since S-192 provided a wider selection of spectral bands than did ERTS, a comparison of the utility of S-192 and of ERTS data would reveal the improvement in performance through use of more nearly optimum spectral bands.

1.2 SUMMARY OF APPROACH

The approach to assessment of changes in pattern recognition performance caused by variations in atmospheric state was to simulate changes in performance caused by variations in atmospheric optical depth and in terrain base elevation. Then the realism of the simulation was checked by classifying S-192 data collected under known atmospheric conditions and comparing results with those of the model. Three cases were simulated with the model. In the first case, the effects of varying atmospheric visibility at 2,000 ft elevation were assessed In the second and third cases, the effects of varying base elevation

under particular atmospheric states was assessed. A clear atmosphere — high elevation case (40km visibility and 6,000 - 14,000 ft elevation range) and a hazy atmosphere — low elevation case (10km visibility and 2,000 - 6,000 ft elevation) were simulated.

Basically, reflectance signatures of common midwestern crops were calculated from aircraft multispectral data using procedures further described in section 2.3. Then the different atmospheric states and base elevations were simulated, and path radiance, path transmission, and solar and diffuse irradiances calculated using a model developed by Robert Turner [1]. The reflectance signatures were converted to radiance signatures at each of the atmospheric states. A computer program simulating the ERIM linear classifier was written. It was trained on radiance signature sets collected under base atmospheric conditions, then it classified samples taken from the radiance signatures generated for other atmospheric conditions. In this way confusion matrices of performance were generated for several different cases.

The approach to the Cripple Creek study was to prepare a recognition map of terrain features using S-192 data and training sets selected by Dr. Harry Smedes of the U. S. Geological Survey, Denver, Colorado and Jon Ranson, a Colorado State University graduate student assisting Dr. Smedes. From an analysis of training set signature statistics, seven optimum S-192 bands were selected for final mapping. The final map accuracy was assessed and results were compared with a similar effort using ERTS-1 data [10].

1.3 SUMMARY OF CONCLUSIONS AND RECOMMENDATIONS

A simulation study of the effects of atmosphere on the performance of pattern recognition devices was performed. Also, computer assisted land resource mapping was performed on an agricultural scene in Michigan and a natural vegetation scene near Cripple Creek, Colorado S-192 and supporting aircraft data were used for the Michigan study, while only

S-192 data were used for the Colorado study. As a result of these studies, the following conclusions were made:

1) Simulation studies provided an accurate measure of the effects of changes in atmospheric visibility and of base elevation on the classification of agricultural crops. This technique could provide additional useful information if used with atmospheric models of proven validity (such as Turner's) with accurate levels of sensor noise, and with realistic crop or other signature reflectance statistics derived from low and medium altitude aircraft data.
2) In simulation tests of crop recognition accuracy using simulated ERTS bands (which were narrower than the actual ERTS bands) and four "optimum" S-192 bands, with accurate simulations of ERTS and S-192 sensor noise, the four narrowed ERTS bands provided nearly the same performance under training conditions of atmospheric visibility and provided 65% training set recognition accuracy or better over a wider range of visibilities than the four "optimum" bands.
3) Seven optimum channel simulated crop classification performance was marginally better than the four optimum band performance with S-192 noise conditions at the training condition, and performance was more extendable over visibility variations than the four channel results.
4) Under conditions of no sensor noise — with variations in signals caused only by terrain variations — the crop classification results were extendable over larger ranges of visibility and base altitude with the narrowed ERTS bands than with the four or seven optimum bands. This occurred because the ERTS bands were located in a

spectral region where atmospheric effects were reasonably small, while both the seven and four optimum bands included bands in the blue-green portion of the spectrum. In using data from newer spacecraft sensors (with generally higher signal to noise ratios than either ERTS or S-192) for agriculture surveys one should consider band selection (both number and placement) in the light of the extension of signatures over a range of atmospheric conditions rather than solely on the performance in separating training set signatures. The ability to preprocess data is also an important consideration, and the results presented shed some light on how well preprocessing must be performed.

5) Using S-192 data collected in August 1973 over the Michigan Agricultural Test Site near Lansing, corn, woods, bare soil, and soybeans were mapped with 71.1, 81.4, 85.7, and 50.0% accuracy respectively. The low performance on soybeans is attributed to sparse crop cover as a result of extremely late planting in the 1973 growing season.

6) In Cripple Creek, Colorado land resource mapping, six optimum bands were chosen from the thirteen available S-192 bands. The bands selected were narrowed versions of the four ERTS bands plus two bands in the 1.5 - 2.35 μm region of the spectrum. The thermal band was not selected even though the data were collected near midday, probably because of the relatively high 2.3°K noise equivalent temperature (NET) in the thermal band.

2

ASSESSMENT OF ATMOSPHERIC EFFECTS ON PATTERN RECOGNITION PERFORMANCE

This section contains a discussion of the portion of this project dealing with the assessment of effects of variation in atmospheric optical depth and of variation in terrain elevation on the performance of a pattern recognition algorithm. The basic rationale for such a study has been presented in section 1.1. This section focuses on procedures, analysis of results, and discussion of implications of those results.

2.1 APPROACH

The approach to this effort has already been summarized in section 1.2. In this section, the approach is documented in more detail. Figure 1 schematically details the approach.

First, we generated reflectance signatures of various midwestern crops to use in further simulation studies. These were generated from aircraft multispectral scanner data collected at the same time as the Skylab SL-3 overflight of the Michigan test site on 5 August 1973. Data from the ERIM M-7 scanner were smoothed to simulate 80m resolution, and in the process, reduce digitized sensor noise to negligible proportions. Then the data were calibrated to reflectance by use of reflectance panel and secondary reflectance standards. Finally reflectance signatures for the common crops in the scene were generated. See Section 2.2. Wavelengths of the M7 scanner channels are given in [6].

The atmospheric model of Robert Turner was used to generate path radiance and transmission and total irradiance for a variety of atmospheric visibility and base elevation conditions. Calculations were made for the centers of the ERIM M-7 scanner bands. A 2,000 ft elevation study of variations of atmospheric parameters with variations

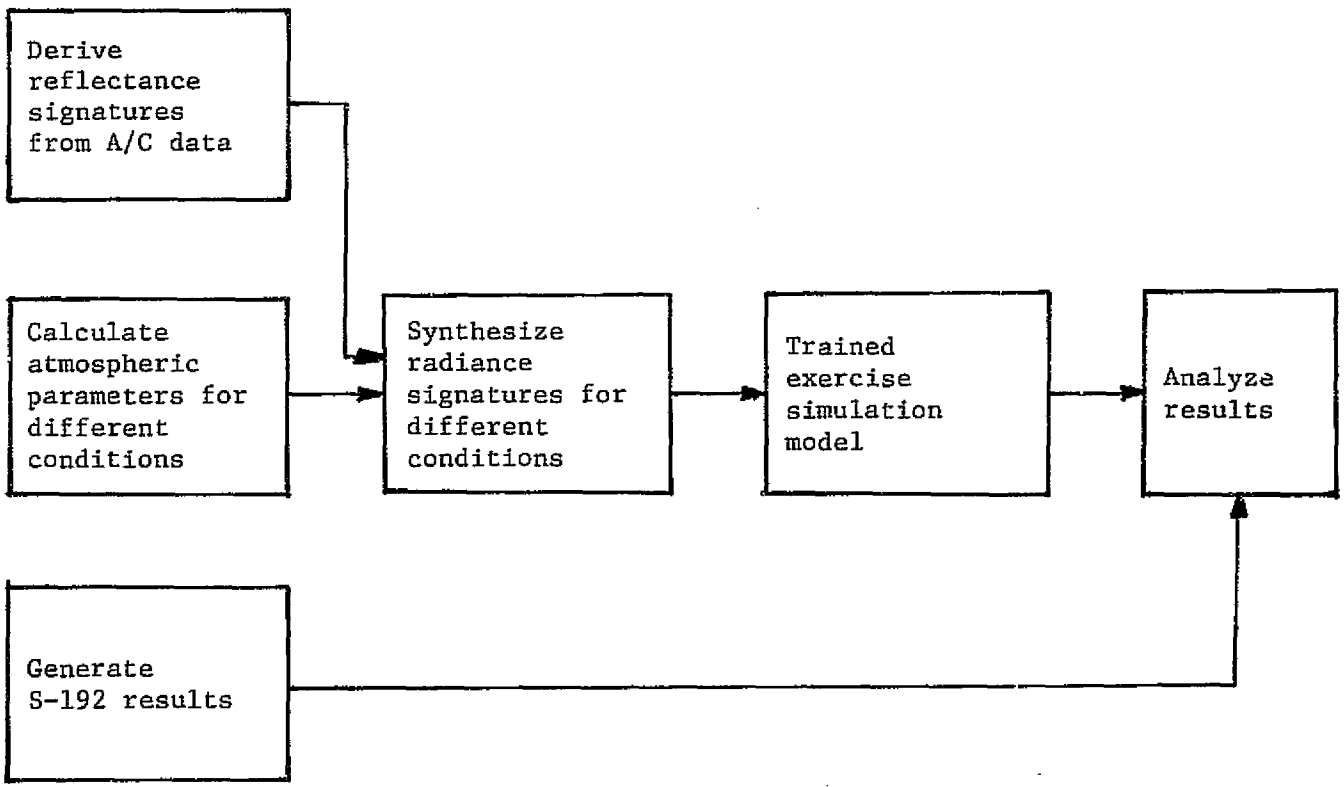

FIGURE 1. FLOW OF ATMOSPHERIC EFFECTS STUDY

in visibility was performed. Also, two base elevation variation studies were performed. For 10km visibility the base elevation was varied from 2,000 - 6,000 ft while for 40km visibility the base elevation was varied from 6,000 - 14,000 ft. See Section 2.3.

After calculating atmospheric parameters for a variety of atmospheric and base elevation conditions, these data were used to calculate crop radiance signatures for the crops whose reflectance signatures had been previously calculated. The radiance signatures, simulations of what a sensor would see under these atmospheric conditions, were used in a model simulating the pattern recognition device. We used the model to calculate the performance of the pattern recognition device, assuming it had been trained on signatures collected under one atmospheric condition. Confusion matrices were generated showing performance as a function of atmospheric state and base elevation. Since these results were generated using data generated from training sets only, we refer to these results as "training set" results. To simulate effects of sensor noise on classification, two simulations were run. The first was run on noise-free data and the second was run on data in which the effects of sensor noise had been included. See Section 2.4.

S-192 data from the Michigan Test Site area were classified, using nearly the same categories as for the simulation study. Atmospheric measurements made at the time of Skylab overpass were used to determine the atmospheric state. Results of evaluating the Skylab map accuracy were compared with model results to determine model validity. See Section 2.6.

Last, analysis of the results was done to assess the range of variation in base elevation and atmospheric state over which good pattern recognition performance could be retained. See Section 2.5.

2.2 AIRCRAFT DATA PROCESSING

The purpose of processing aircraft data collected in support of the Skylab overpass was to derive directional reflectance signatures

for use in the model described in Section 2.4. For this purpose, data collected at 1,000 and 10,000 ft over the Michigan Test Site were used. The data were collected on 5 August 1973 at 0830-1130 EDT.

The starting point for analysis was 10,000 ft data already digitized and converted to 7094 computer compatible format and 1,000 ft data digitized and scaled but not yet converted to ERIM 7094 format. See Figure 2 for a flow of aircraft data processing operations.

2.2.1 1,000 FT DATA PROCESSING

Data were first converted to 7094 format to facilitate further processing. Then, using graymaps already generated for CDC 1604 computer processing steps (on another project), the locations of each of the gray reflectance panels and of the secondary standards were found.

Signatures for each of the panels and for the standard fields were extracted using the STAT program. The next step was a calibration of each channel of data in terms of reflectance, using panels signatures and panel reflectance values from report 101700-10-X [3]. As shown in Figure 3 the panel means (in integers) were plotted versus the panel reflectances and a best fit regression line determined for the data. Two constants, an additive constant a and a multiplicative constant b were determined such that:

$$\text{reflectance} = a + b\ (\text{integer value}) \tag{1}$$

These constants were determined so as to minimize the mean square error of the fit of the line relating panel signals to reflectance.

Once the constants a and b were chosen for each spectral channel, the reflectances of each of the secondary standard fields (used to calibrate 10,000 ft data) were determined through an application of equation 1.

2.2.2 10,000 FT DATA PROCESSING

The processing of the 10,000 ft data began with a smoothing of the basic data to 80m resolution. The data were digitized with 14.4m

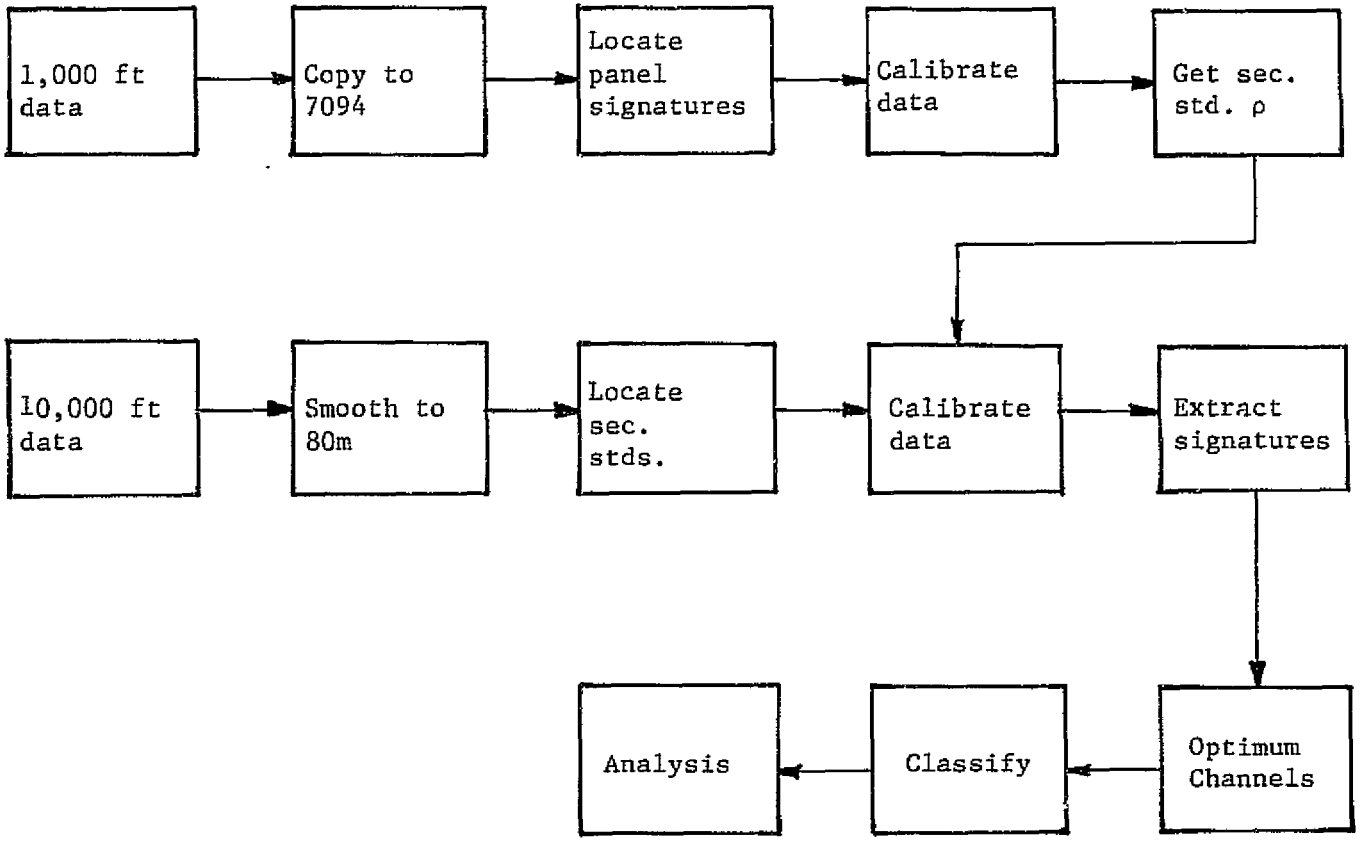

FIGURE 2. FLOW OF AIRCRAFT DATA PROCESSING

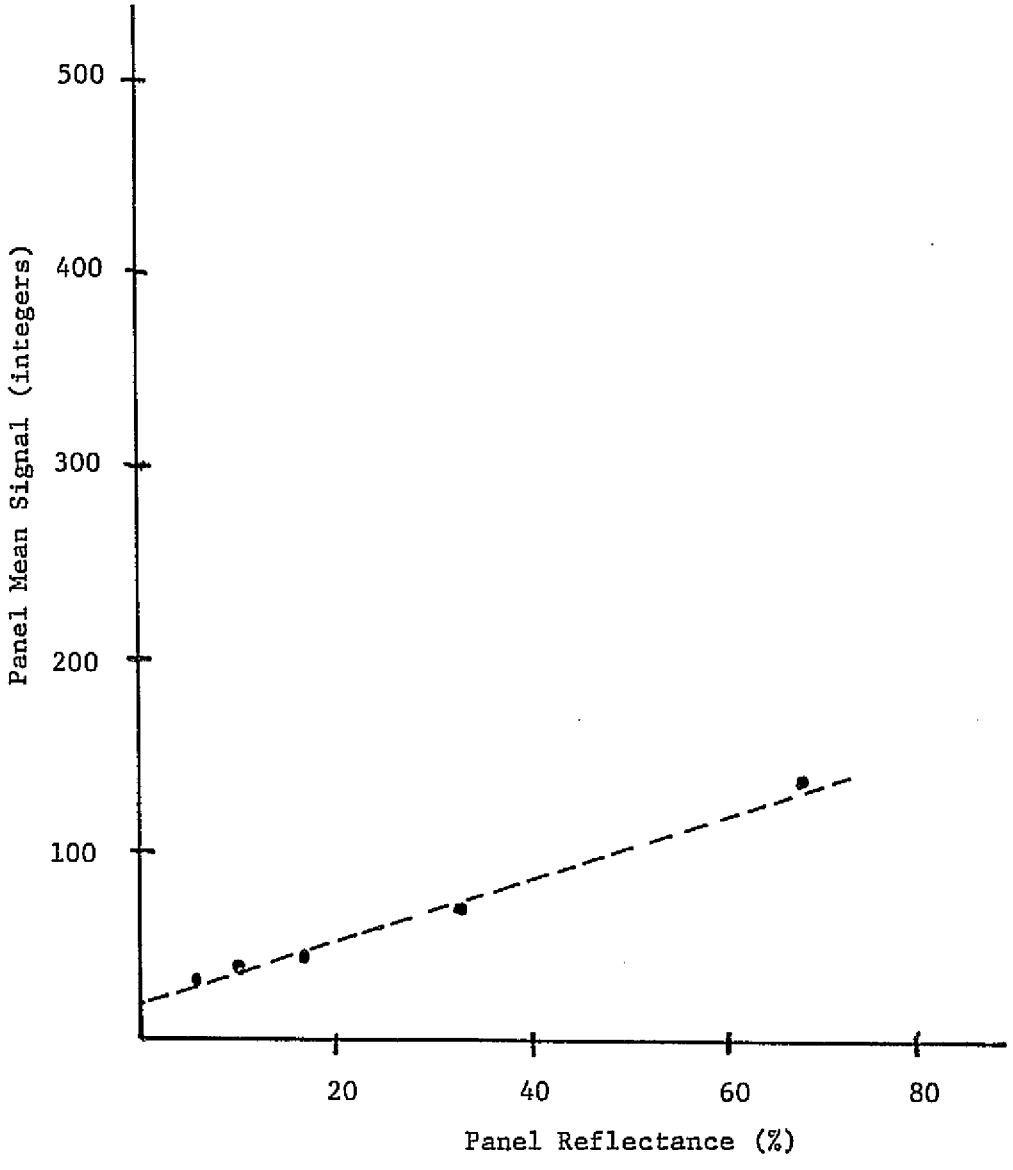

FIGURE 3. TYPICAL PLOT OF PANEL SIGNALS VERSUS REFLECTANCE (line shown is best fit)

resolution along the scan line and 12.19m resolution along the flight line. To smooth to a square 80m element required a smoothing operation of 6 x 7 across the scan line and along the flight line respectively.

After the data were smoothed to about 80m (the actual figures are 86.4 x 85.3m), the same secondary standard fields located on the 1,000 ft data were found on a 1 x 1 graymap of a red band and the signatures obtained. Then a calibration of the data was performed by determining constants a and b relating digital counts to reflectance in exactly the same way as was done for the reflectance panel data in the 1,000 ft data set. Separate a and b values were obtained for each spectral channel.

The next step was the extraction of signatures from large fields for the crop types bare soil, trees, corn, soybeans, oats, pasture, stubble, dense green, and water. Large field data were used so that the same fields can be located on Skylab data. Multiple samples of each category of crop were selected and signatures extracted from the combined area.

During the combining step, the results were scaled to reflectance by imposing the scaling coefficients (the b values previously determined) in the combining operation. Later revised mean value cards (representing the difference between the scaled mean and the constant a) were punched and inserted in the signature deck.

The results of the aircraft data processing, the reflectance signatures, are shown in Table 1. Shown there are mean values and standard deviations for the nine crop types previously mentioned. In interpreting these results, one should remember that these signatures represent the appearance of crops at 80m resolution. Also, at the extreme values of smoothing used on the original aircraft data, the standard deviations shown represent the variation in the reflectance of the training sets; the sensor noise also present on the analog tape recorded data was reduced to negligible proportions by the extensive smoothing of the data.

TABLE 1

REFLECTANCE MEANS AND STANDARD DEVIATIONS
FOR MICHIGAN AGRICULTURE CROPS — 5 AUGUST 1973

(standard deviations in parentheses)

Class	.41 - .48 1	.46 - .49 2	.48 - .52 3	.50 - .54 4	.52 - .57 5	.55 - .60 6	.58 - .64 7	.62 - .70 8	.67 - .94 9	1.0 - 1.4 10	1.5 - 1.8 11
Dense Corn	2.65 (.276)	3.07 (.264)	2.91 (.237)	4.17 (.297)	5.62 (.502)	5.31 (.471)	4.39 (.313)	3.45 (.225)	30.47 (3.36)	37.02 (2.85)	14.54 (1.18)
Woods	1.68 (.737)	1.65 (.674)	1.52 (.575)	2.37 (.614)	3.55 (.739)	3.02 (.804)	2.20 (.757)	1.56 (.609)	25.06 (.368)	33.24 (.416)	11.51 (.244)
Bare Soil	10.41 (3.58)	11.30 (3.97)	10.59 (3.60)	12.27 (3.58)	13.20 (3.75)	15.63 (4.34)	15.74 (4.52)	15.63 (4.29)	20.05 (7.78)	29.65 (9.44)	33.82 (6.90)
Sparse Corn	3.63 (.753)	3.96 (.902)	3.73 (.765)	5.51 (.755)	7.58 (.891)	7.29 (1.04)	5.80 (1.19)	4.53 (1.12)	29.12 (3.36)	36.39 (4.50)	18.90 (3.00)
Stubble	4.45 (.429)	5.44 (.572)	5.22 (.592)	7.17 (.607)	9.26 (.544)	10.00 (.793)	9.76 (1.18)	8.81 (1.31)	24.50 (2.34)	37.60 (3.91)	30.96 (4.17)
Ripe Oats	2.67 (.486)	3.56 (.456)	3.51 (.371)	4.90 (.538)	6.26 (.823)	7.01 (.805)	7.54 (.577)	7.23 (.528)	14.86 (3.03)	21.66 (3.07)	15.35 (.924)
Soybeans	5.08 (.953)	5.46 (1.25)	4.94 (1.16)	6.73 (1.32)	9.12 (1.24)	8.94 (1.63)	7.49 (.198)	6.08 (2.13)	3.99 (5.52)	48.16 (5.06)	29.94 (3.19)
Dense Green	2.87 (.340)	3.07 (.296)	2.78 (.298)	4.45 (.516)	6.73 (.700)	5.92 (.801)	4.03 (.654)	2.70 (.502)	41.36 (3.03)	48.08 (4.06)	20.56 (2.62)
Pasture	3.68 (.136)	4.16 (.111)	3.84 (.203)	5.57 (.240)	7.51 (.510)	7.60 (.333)	6.69 (.549)	5.54 (.858)	23.06 (7.11)	34.41 (5.79)	20.16 (2.19)

The reflectances of materials shown in Table 1 are in qualitative agreement with reflectance spectra in the Earth Resources Spectral Information System (ERSIS) and with plant canopy reflectance calculations made by Suits [4]. The calculations of reflectance are thus felt to be accurate.

2.3 TURNER MODEL CALCULATIONS

To determine the effects of changing atmosphere optical thickness and of varying base altitude on ground irradiance, atmospheric transmission, and path radiance, calculations were made using R. Turner's radiative transfer model. The model calculates these radiometric quantities and others given inputs of solar elevation and azimuth, view angles, atmospheric state, and background albedo. Atmospheric state is specificed as an optical thickness at various wavelengths for which the calculations are to be made.

For the model calculations, the view angle considered was nadir, corresponding to the satellite case. The wavelengths used were the center wavelengths of the ERIM M-7 scanner channels, as shown in Table 1. The solar elevation angle was that for the Michigan data (5 August 1973 at 1130 EDT). A green vegetation albedo was assumed for the background. We assumed various atmospheric optical depths at constant base altitude, then varied the base altitude at two of the atmospheric optical depths. Table 2 presents the base altitude cases considered for the atmospheric states presented in the table. The intent of these cases was to cover reasonable situations. Thus the 3-160km sea level case for atmospheric visibility spans almost the entire range of reasonable remote sensing situations. The altitude variations are for an east coast US area (Case 1) and a Rocky Mountains area (Case 2).

The atmospheric state input to the Turner model for the cases shown in Table 2 is straightforward — one needs only to specify the

TABLE 2

ATMOSPHERIC STATES CONSIDERED
FOR TURNER MODEL CALCULATIONS
(EXPRESSED AS HORIZONTAL VISIBILITY)

Case	Horizontal Visibility (km)
1	3
2	6
3	10
4	20
5	40
6	160

Base elevation - sea level

horizontal visual range and the model will make the calculation of atmospheric optical depth at any specified wavelength. For cases shown in Table 3, some modified form of input was required. We simulated the effects of varying base elevation on atmospheric parameters, assuming a constant atmospheric state. Because less air is contained in paths to base elevations above sea level than in paths to sea level, the atmospheric optical depth will be less, even though the horizontal visibility at sea level is unchanged. Thus optical depths for base elevations greater than sea level need to be modified over the sea level case.

For the purpose of these computations, we calculated the Rayleigh optical depth as a direct function of the absolute atmospheric pressure at the altitude in question. Thus, to obtain the Rayleigh optical depth for a base elevation other than sea level, the sea level optical depth is modified by:

$$\tau_h = \tau_o \quad \frac{P_h}{1013} \tag{2}$$

where

τ_h = atmospheric Rayleigh optical depth at base elevation h

τ_o = atmospheric Rayleigh optical depth at sea level

P_h = absolute pressure at elevation h in millibars

The aerosol term was calculated for varying altitudes by reference to the Elterman Standard atmosphere [2]. This standard atmospheric profile is the one used in the Turner model when atmospheric visibilities are used to characterize the atmospheric state. Then the total optical depth was calculated as the sum of the aerosol term, the Rayleigh term, and a term representing ozone absorption.

TABLE 3

BASE ALTITUDE CONDITIONS FOR TURNER MODEL CALCULATIONS

Case 1 — 10km horizontal visibility

Sub Case	Base Elevation (ft)
A	0*
B	2000
C	4000
D	6000
E	8000

Case 2 — 40km horizontal visibility

Sub Case	Base Elevation (ft)
A	0*
B	6000
C	8000
D	10000
E	12000

*represents cases shown in Table 2

2.3.1 DISCUSSION OF RESULTS

After the optical depths had been calculated for each case, the Turner model was exercised on the IBM 370 computer. Results of the calculations are shown in Figures 4 and 5. Figure 4 shows the reflectance signature multiplicative term, $\frac{E\tau}{\pi}$ and the additive term L_p as a function of visibility from 3 to 160km visibility. Curves for 0.52 and 0.66 μm are shown to illustrate the different behavior of these terms for different wavelengths. As can be seen from Figure 4, the multiplicative term increases as visibility increases. This occurs because the path transmission from ground to satellite increases as the visibility increases. The total irradiance remains nearly constant. In Figure 4, the path radiance decreases as the atmospheric visibility increases. This occurs because there is less scattering at high atmospheric visibility than at low visibilities.

Figure 5 shows the variations of signature multiplicative and additive terms with base altitude at an atmospheric visibility of 10km. Again, the curves for 0.52 and 0.66 μm are shown. Referring to Figure 5, as base altitude increases, the horizontal visibility increases. The horizontal visibility increases because there is less scattering at elevations above ground level. Thus the multiplicative term increases with base altitude both because irradiance increases and because path transmission increases. Referring to Figure 5, the path radiance term decreases as base elevation increases because of reduced scattering.

Because the multiplicative term increases with increasing visibility or base altitude and the additive term decreases, the signature means for various classes may either increase, decrease, or remain nearly constant, depending on the reflectance in a particular band. Low reflectance class means will decrease with increasing visibility or base altitude because of the dominance of the additive term. The converse is true of high reflectance classes because of the dominance of the multiplicative term.

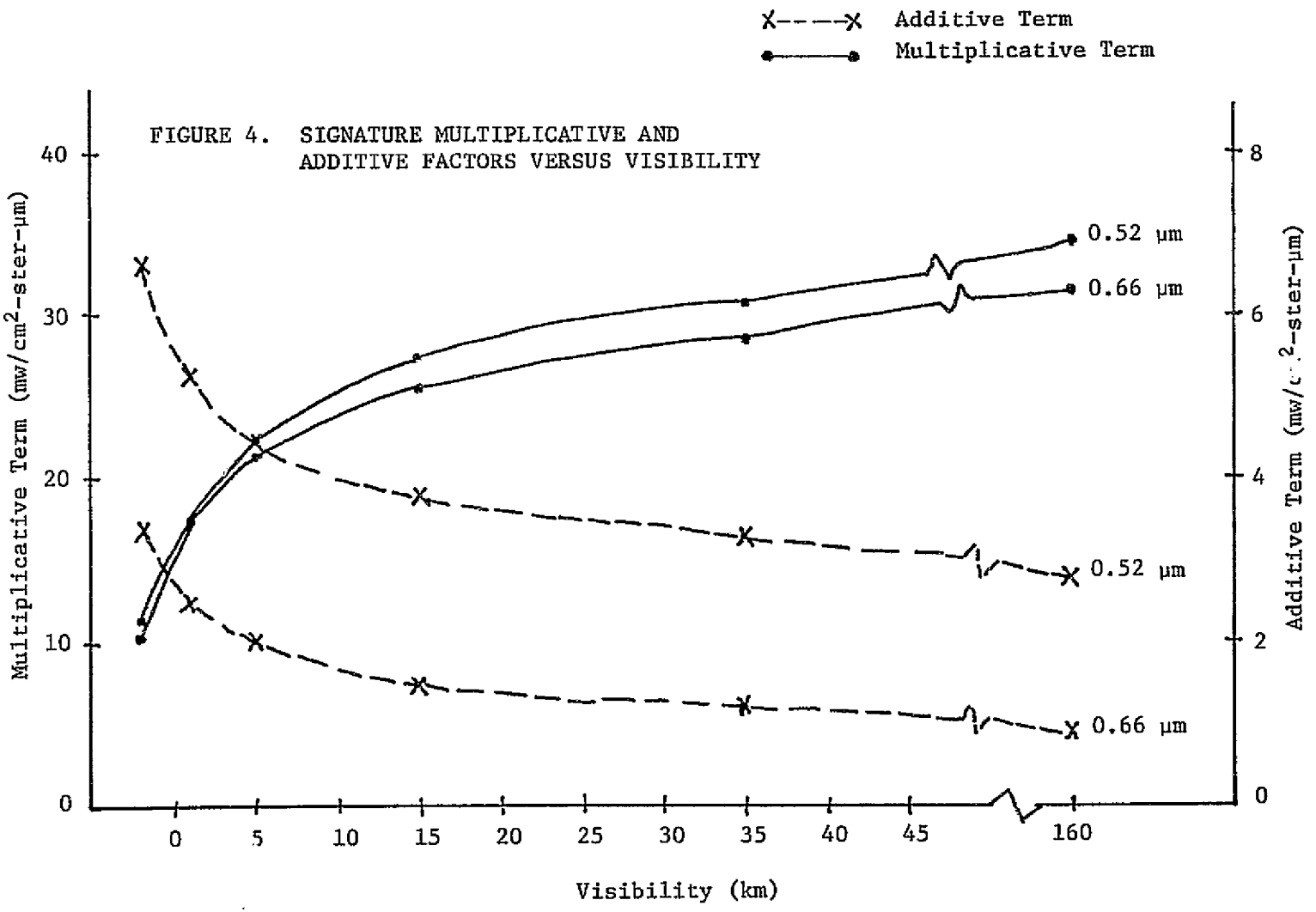

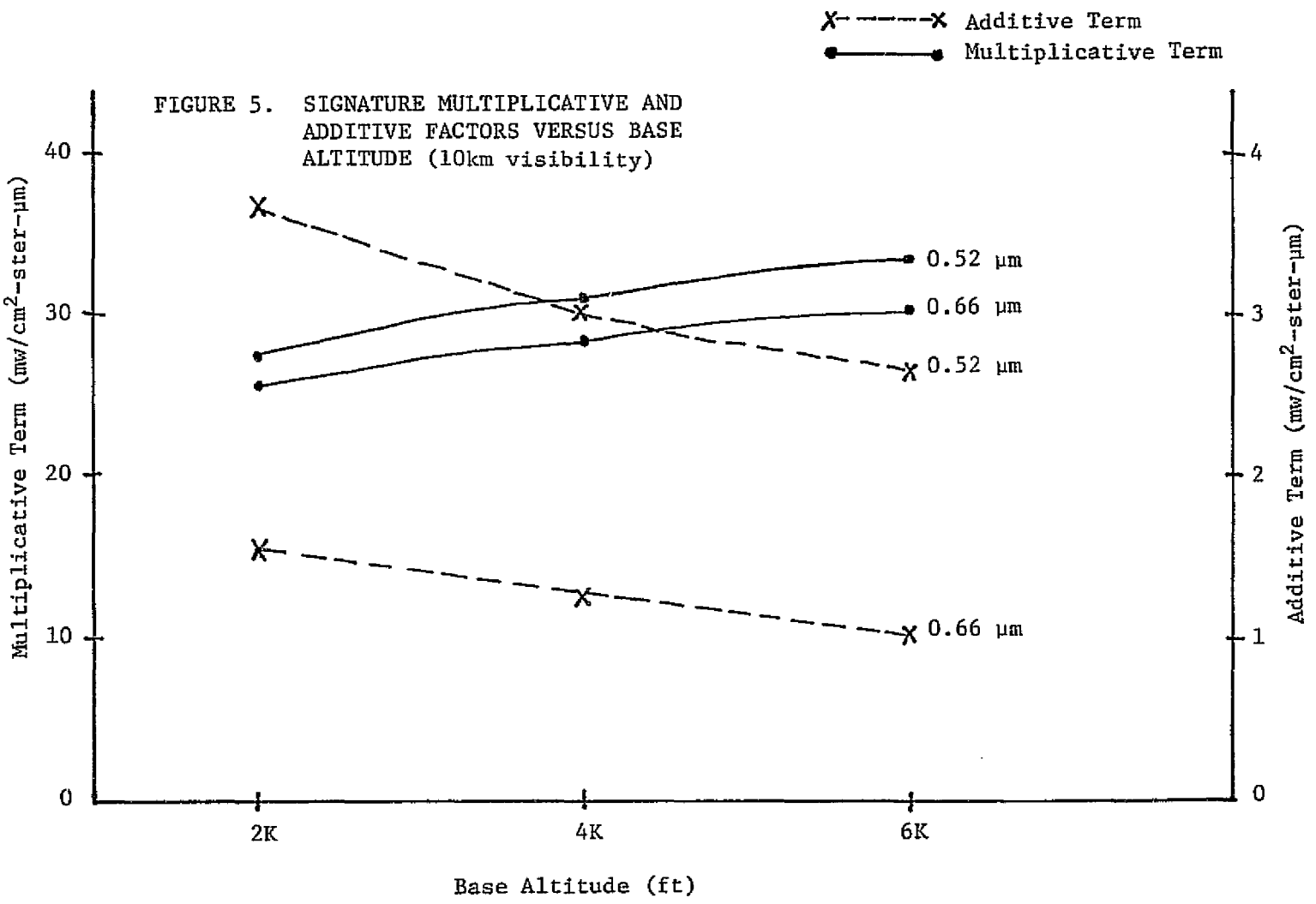

FIGURE 5. SIGNATURE MULTIPLICATIVE AND ADDITIVE FACTORS VERSUS BASE ALTITUDE (10km visibility)

2.3.2 SIGNATURE TRANSFORMATION

Reflectance signatures calculated from aircraft data were transformed, using the Turner model calculations previously discussed, to create radiance signatures under various atmospheric visibility and base altitude conditions. Radiance signatures are extracted from sensor data.

Three types of signature transformation were employed. First, signature mean values were converted from reflectance to radiance by the formula:

$$L = \frac{E\tau\rho}{\pi} + L_p \qquad (3)$$

where

L = signature radiance mean [mw/cm^2-ster-μm]

E = total downward irradiance from Turner model [mw/cm^2-ster-μm]

τ = path transmission from ground to sensor

ρ = signature reflectance mean value

L_p = path radiance calculated by Turner model [mw/cm^2-ster-μm]

All variables in equation 3 were functions of wavelength, and the calculation was carried out for each of the scanner bands, using Turner model values calculated at the center wavelength of the bands.

The covariance terms of the reflectance signatures were transformed by the formula:

$$V_{mn} = \rho_{mn} \frac{E_m E_n \tau_m \tau_n}{\pi^2} \qquad (4)$$

where

V_{mn} = the covariance between the radiance in spectral bands m & n

ρ_{mn} = the covariance between the reflectance in spectral bands m & n

E_m = total irradiance in band m

τ_m = path transmission in band m

The noise of the sensor was introduced by the formula:

$$U_{kk}^2 = V_{kk}^2 + N^2 \qquad (5)$$

where

U_{kk}^2 = the transformed variance of channel K

V_{kk}^2 = the radiance variance of channel K, calculated from equation 4

N^2 = the mean square sensor noise as deduced from performance reports

The simulation of scanner noise assumes that the scanner noise is uncorrected with variations in signature radiance.

2.4 SIGNATURE MODIFICATION MODEL DEVELOPMENT AND EXERCISE

2.4.1 MODEL DEVELOPMENT

As stated in the introduction to Section 2, the approach taken to study of atmospheric effects on pattern recognition devices was modelling. Computer software for the 7094 computer was developed to read a signature deck and generate a sample of specified size from that distribution. Then the samples are classified, using the ERIM linear classifier [5] trained by signatures entered to the model. The model generates a confusion matrix, a display showing how points from the sample distributions were classified by the trained classifier.

2.4.2 MODEL EXERCISE

After the model had been developed and debugged, it was exercised using reflectance signature data from aircraft data analysis transformed by multiplicative and additive terms as previously discussed. Three broad cases of atmospheric effects were considered — ERTS-1 effects (4 channels), S-192 effects (best 7 channels), and S-192 (best 4 channels). For each case the effects of change of atmospheric visibility from 3 to 160km (training on data with 10km visibility) were

assessed. Two cases of variation in performance with base elevation changes were assessed — a variation from 2,000 to 8,000 ft (training on 2,000 ft base elevation signatures) and a variation from 6,000 to 14,000 ft (training on 8,000 ft data). The 2,000 to 8,000 ft test was conducted at 10km visibility (simulating east coast cases) and the 6,000 to 14,000 ft test was conducted at 40km visibility (simulating west coast cases). These cases are summarized in Table 4.

Finally, for each set of wavelengths and visibility or base elevation conditions two cases were computed — one with sensor noise (ERTS or S-192 as appropriate) and one without. Results will be discussed in Section 2.5.

2.5 ANALYSIS OF SIMULATION MODEL RESULTS

As a result of the simulation model calculations, results were generated for four optimum bands, the four ERTS bands, and seven optimum bands. Cases with and without sensor noise were generated to compare the intrinsic separability of the classes with the actual separability under ERTS and S-192 conditions.

2.5.1 FOUR OPTIMUM BAND RESULTS

The four optimum channels, selected on the basis of the separation of the reflectance signatures, were 0.48 - 0.52, 0.55 - 0.60, 0.62 - 0.70, and 1.5 - 1.8 μm.

Figures 6 and 7 show results of the simulation of classifier accuracy versus visibility for noise free and noisy cases respectively. Referring to Figure 6, the probability of correct classification is shown as the solid line. The distance between the solid and dashed line shows the probability of misclassification. The difference between the dashed line and the horizontal line at 1.0 represents the amount not classified. For these plots, a five class recognition problem was assumed. The classes were corn, woods, soil, soybeans, and other; these classes represent those which one would typically classify in satellite data collected over Michigan in August.

TABLE 4

CASES CONSIDERED FOR
CLASSIFICATION MODEL EXERCISE

Case 1 – Effects of Atmospheric Optical Thickness

a. Select 4 bands closest to ERTS
b. Train on 10km data
c. Classify 3, 6, 10, 20, 40, 160km data

Case 2 – Effects of Base Altitude-1

a. Select 4 bands closest to ERTS response
b. Train on 2,000 ft data
c. Classify 2000, 4000, and 6000 cases

Case 3 – Effects of Base Altitude

a. Select 4 bands closest to ERTS response
b. Train on 8,000 ft data
c. Classify 6000, 8000, 10000, and 12000 ft data

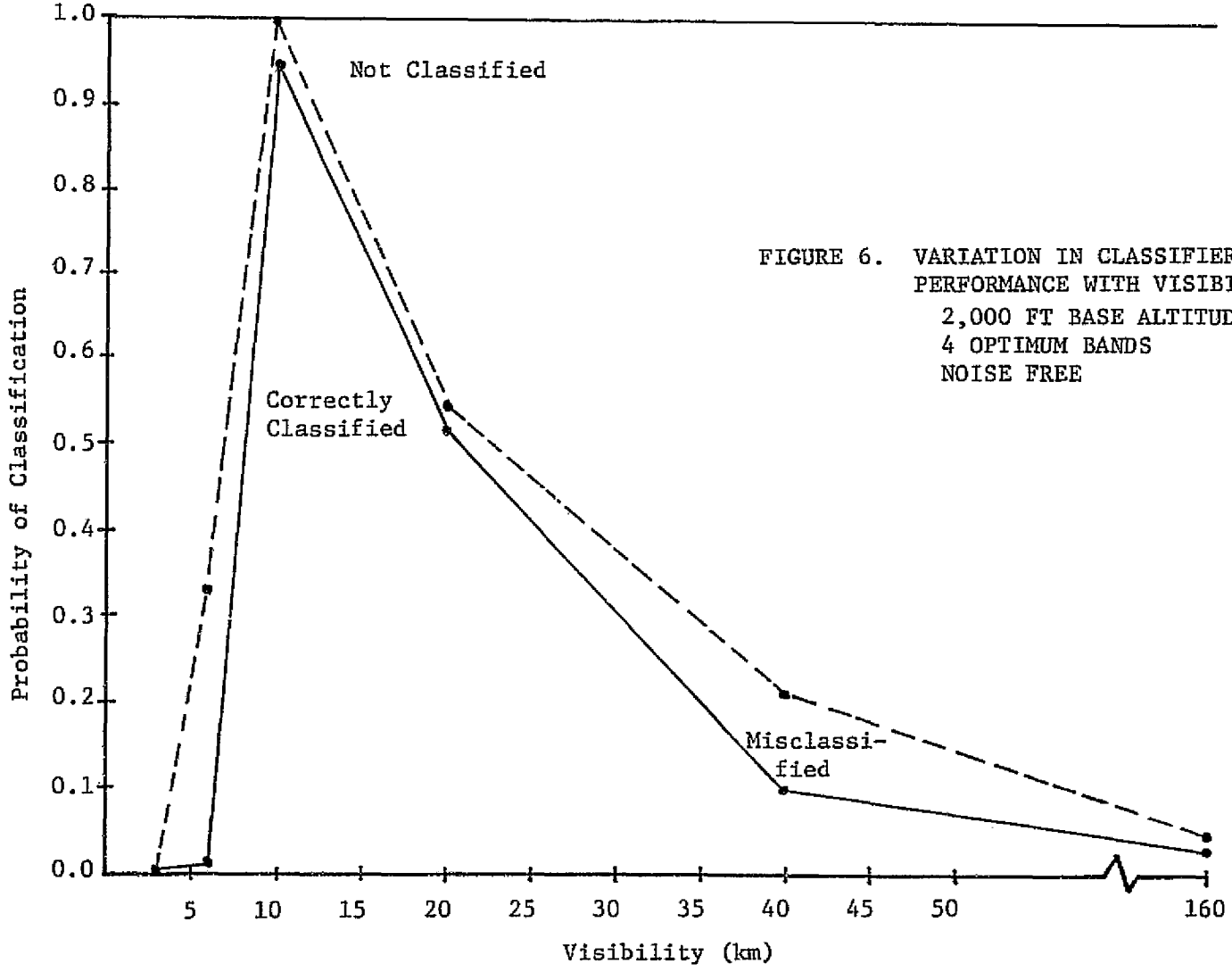

FIGURE 6. VARIATION IN CLASSIFIER PERFORMANCE WITH VISIBILITY
2,000 FT BASE ALTITUDE
4 OPTIMUM BANDS
NOISE FREE

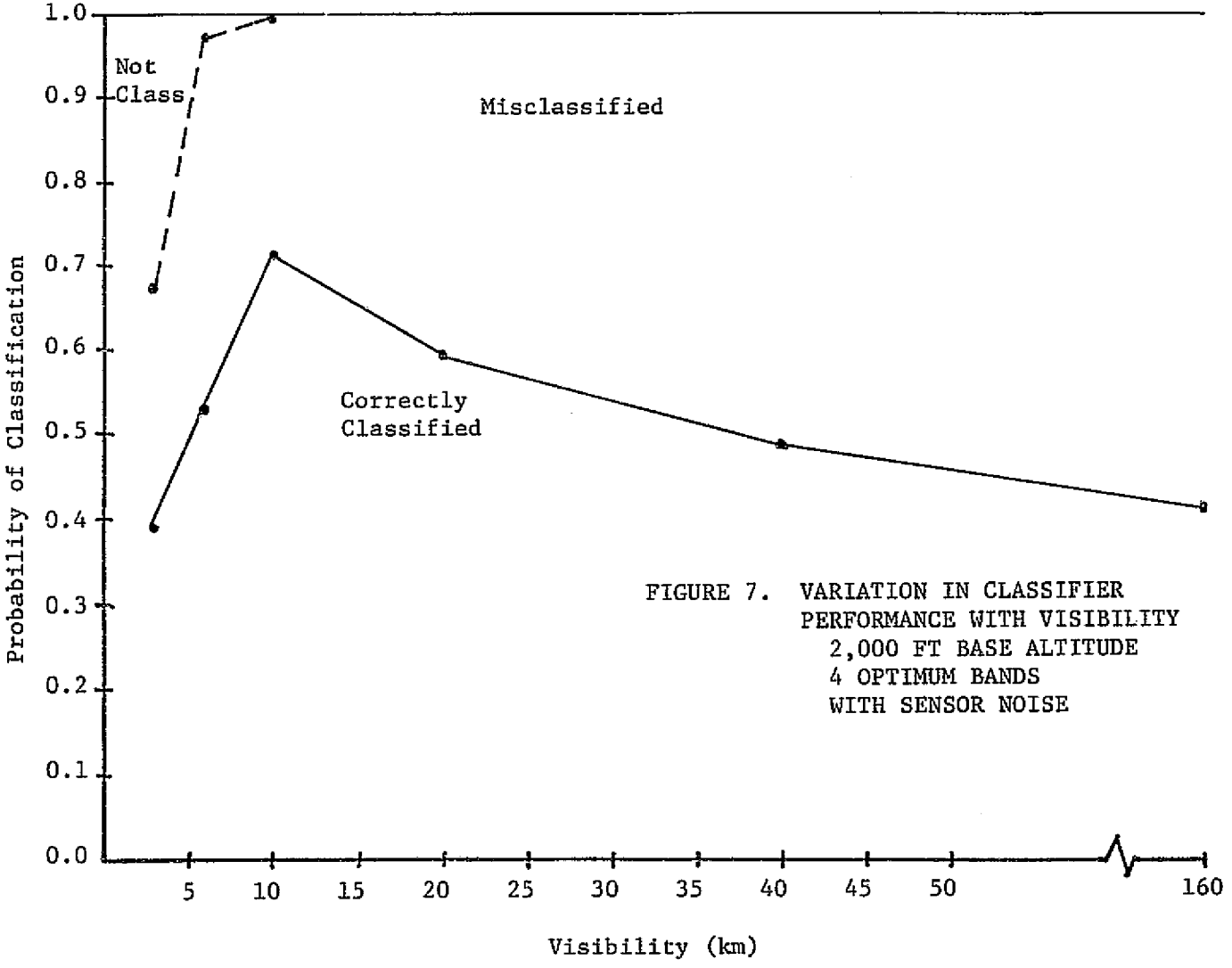

FIGURE 7. VARIATION IN CLASSIFIER PERFORMANCE WITH VISIBILITY
2,000 FT BASE ALTITUDE
4 OPTIMUM BANDS
WITH SENSOR NOISE

Referring to Figure 6, the average probability of correct classification at the training condition at 10km data is 0.942 for the five classes. The probability of correct classification decreases as conditions vary from the training condition. For small changes from the training condition, the major effect is to assign samples to the "not classified" category, rather than to classify.

Comparing Figure 6 to Figure 7, we see that when sensor noise effects are also simulated, the performance degrades from 0.942 to 0.719 probability of correct classification at the training condition. But for the "noisy" case, the reduction in performance as conditions different from the training case are simulated is less severe than for the "noise-free" case because the decision regions for each class are larger. This occurs because each signature has larger variance in each channel as a result of the added sensor noise. The range of visibilities over which the performance is degraded less than 5% from that at the training condition is from 8.97km to 13.9km. Later, these numbers will be compared with similar numbers for the 7 optimum channel case.

Figures 8 and 9 show variations in performance as base elevation is varied from 2,000 to 6,000 ft. Training was done on the 2,000 ft signatures. Qualitatively, the same comments made for variations of visibility apply to the variation of altitude. At 10km visibility, a variation of base elevation from 2,000 to 2,390 ft causes a degradation of performance of 5% over the training condition.

Figures 10 and 11 show similar curves for variations of altitude from 6,000 to 14,000 ft at 40km atmospheric visibility. In this case, performance is nearly constant over the range of altitudes. Slightly better performance is obtained away from the training condition because of improvement in the recognition of the "corn" and "other" classes. Improved recognition results because these classes were composites of two and four separate training sets respectively. As altitude varied, the recognition accuracy of each of the subclasses

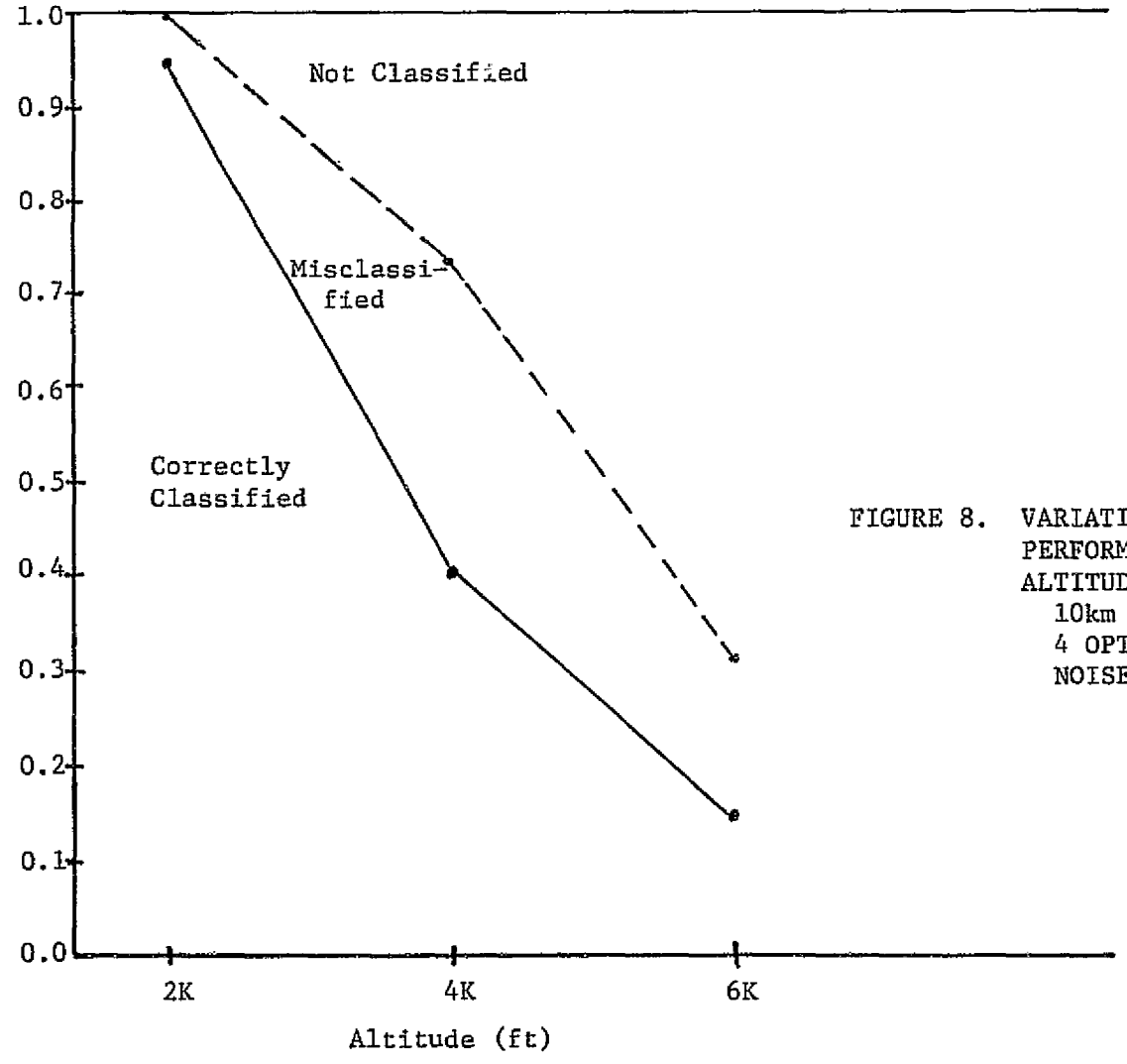

FIGURE 8. VARIATION IN CLASSIFIER PERFORMANCE WITH BASE ALTITUDE
10km VISIBILITY
4 OPTIMUM BANDS
NOISE-FREE

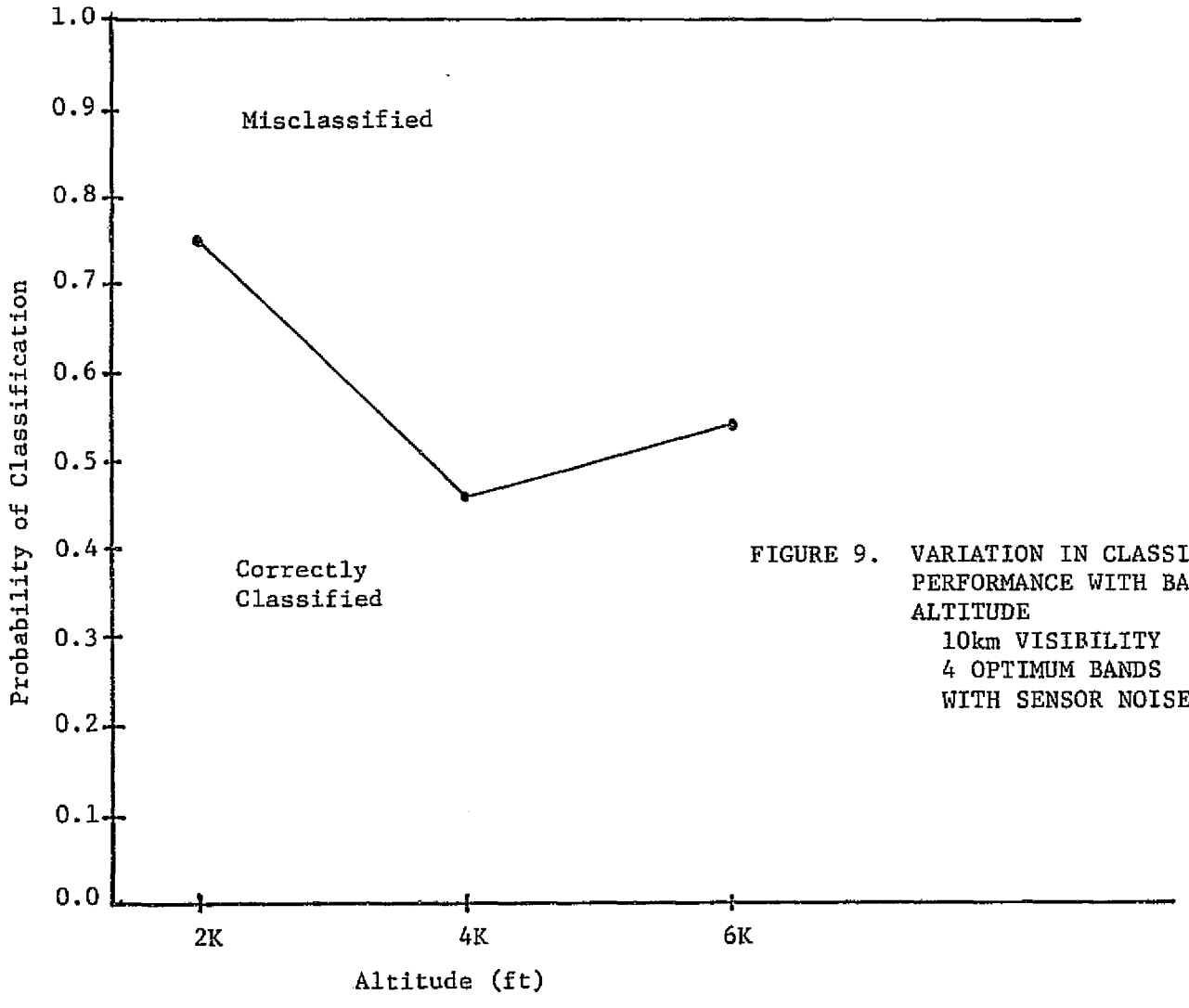

FIGURE 9. VARIATION IN CLASSIFIER PERFORMANCE WITH BASE ALTITUDE
10km VISIBILITY
4 OPTIMUM BANDS
WITH SENSOR NOISE

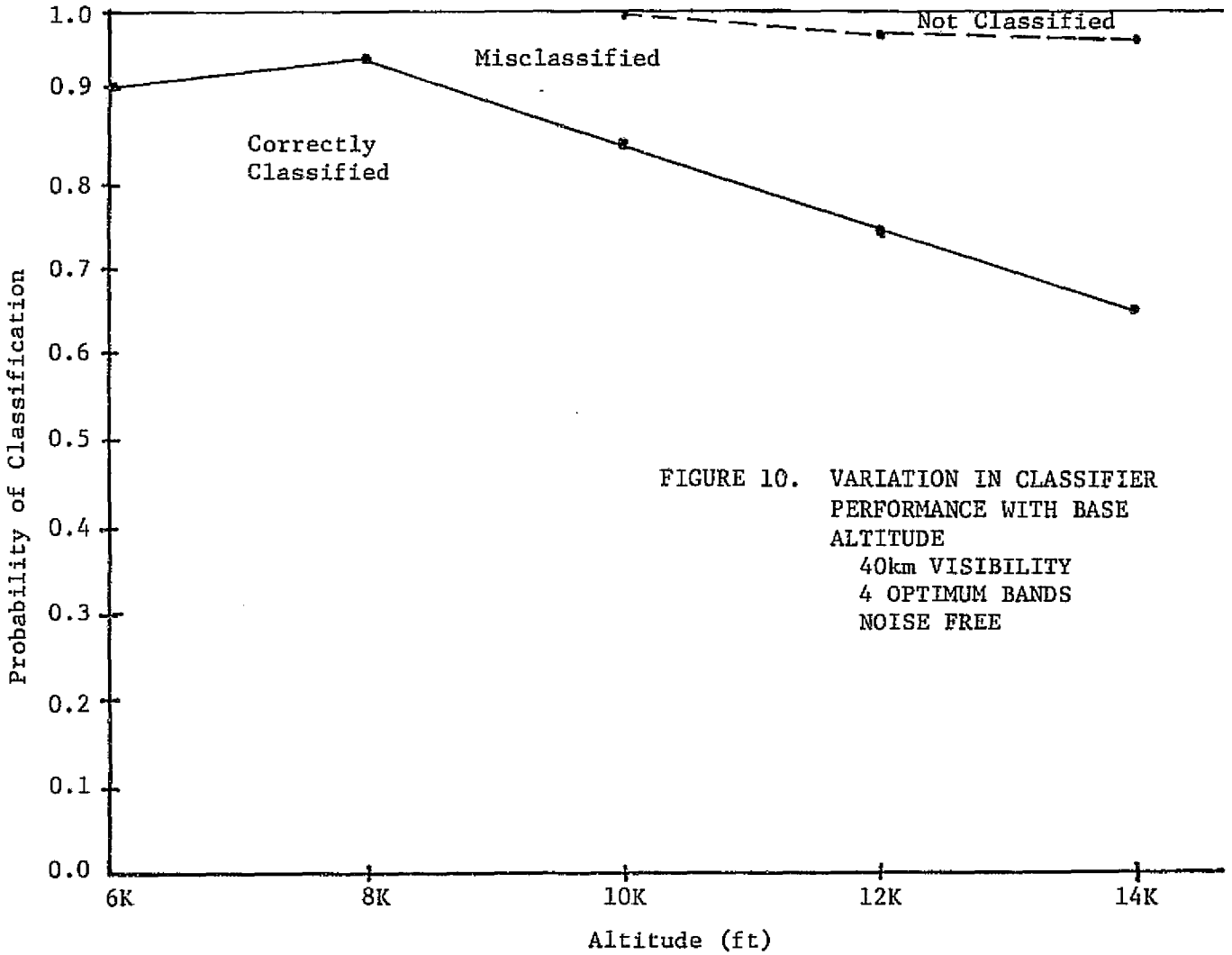

FIGURE 10. VARIATION IN CLASSIFIER PERFORMANCE WITH BASE ALTITUDE
40km VISIBILITY
4 OPTIMUM BANDS
NOISE FREE

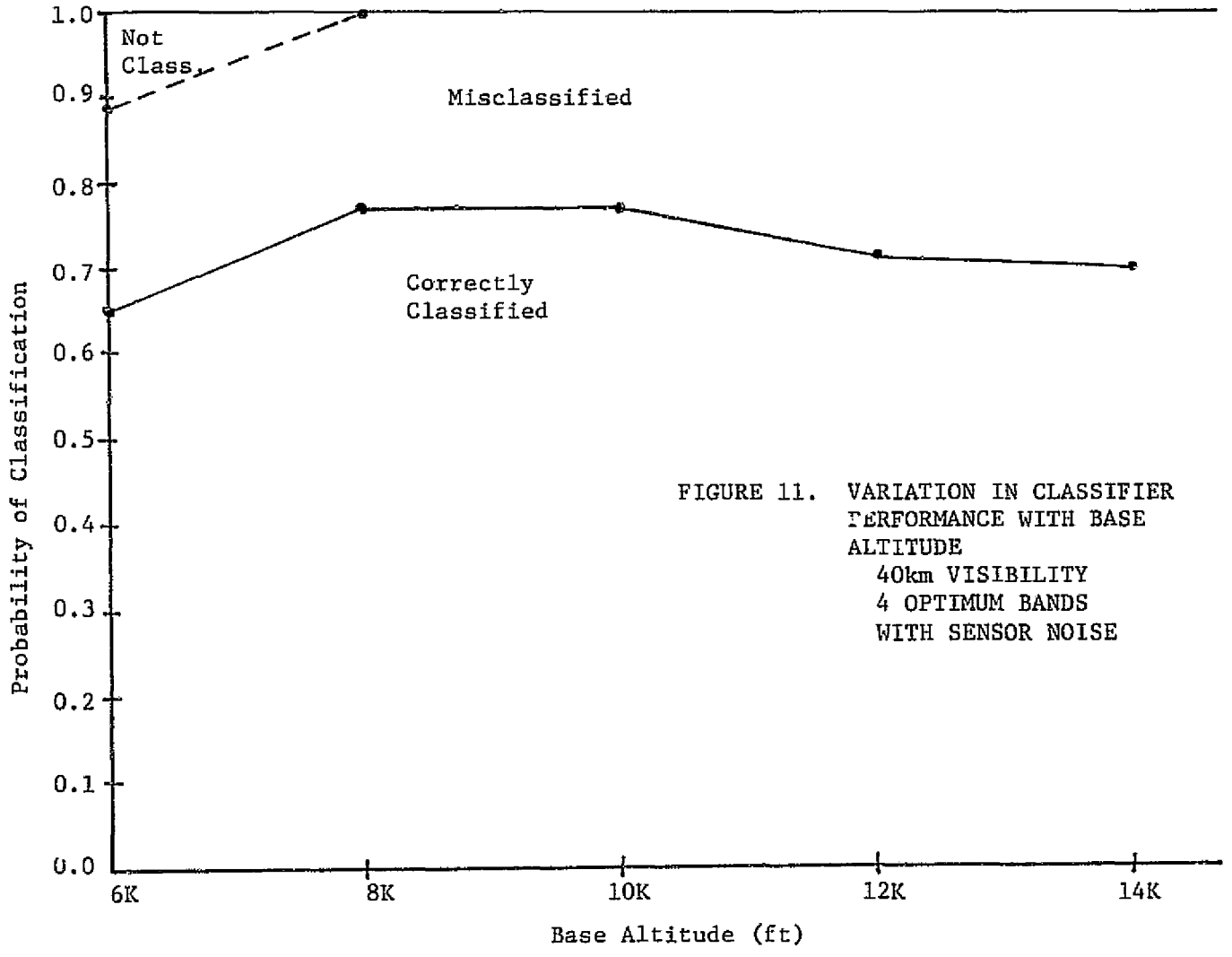

FIGURE 11. VARIATION IN CLASSIFIER PERFORMANCE WITH BASE ALTITUDE
40km VISIBILITY
4 OPTIMUM BANDS
WITH SENSOR NOISE

and the misrecognitions of one subclass as another varied in such a way as to make the overall accuracy inprove slightly for conditions different from the training condition. This would not have occurred if these had been single training sets for corn and other.

2.5.2 FOUR CHANNEL ERTS RESULTS

Figures 12 and 13 show the noise-free and the noisy simulations of recognition accuracy for four bands simulating the ERTS-MSS response. These bands were 0.52 - 0.57, 0.62 - 0.70, 0.67 - 0.94, and 1.0-1.4 μm. The wide bandwidth ERTS-MSS channels were only partially simulated by the narrower M-7 scanner spectral bands. An attempt was made to select M-7 bands close to the ERTS-MSS bands. Because the wide spectral bandwidth was not perfectly simulated, the ERTS results to be discussed in this section should be viewed with caution. Figures 12 and 13 show the same qualitative behavior as Figures 6 and 7. As we move away from the training conditions, the average probability of correct classification monotonically decreases and the average probability of misclassification increases. The performance at the training condition for ERTS and four optimum bands was nearly the same, under noise-free conditions, 0.938 and 0.942 probability of correct classification, respectively. But when sensor noise was simulated the performance of the ERTS was 0.817 while the performance of the four optimum S-192 bands was only 0.719. This is a consequence of the relatively lower noise levels in ERTS as opposed to S-192 data.

The behavior of performance or visibility is varied away from the training condition is similar for the ERTS and four optimum channel cases. Visibility variations from 8.97km to 13.9km produced 5% degradations in the performance of the classifier for four optimum channels. The corresponding numbers for the ERTS case are 9.44 - 12.7km. The slightly larger range of acceptable performance of the four optimum channels is bought at the expense of lower performance at the training condition.

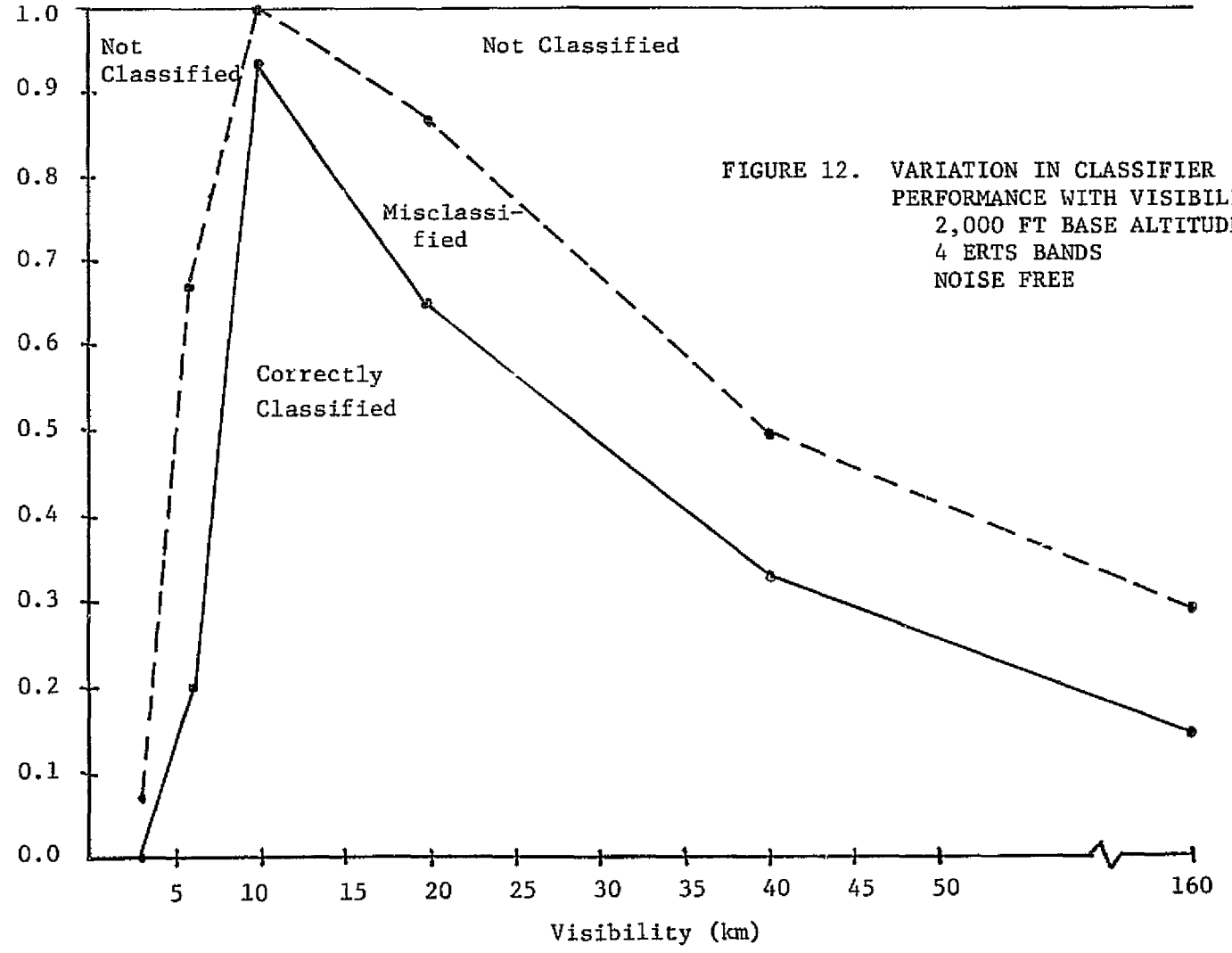

FIGURE 12. VARIATION IN CLASSIFIER PERFORMANCE WITH VISIBILITY
2,000 FT BASE ALTITUDE
4 ERTS BANDS
NOISE FREE

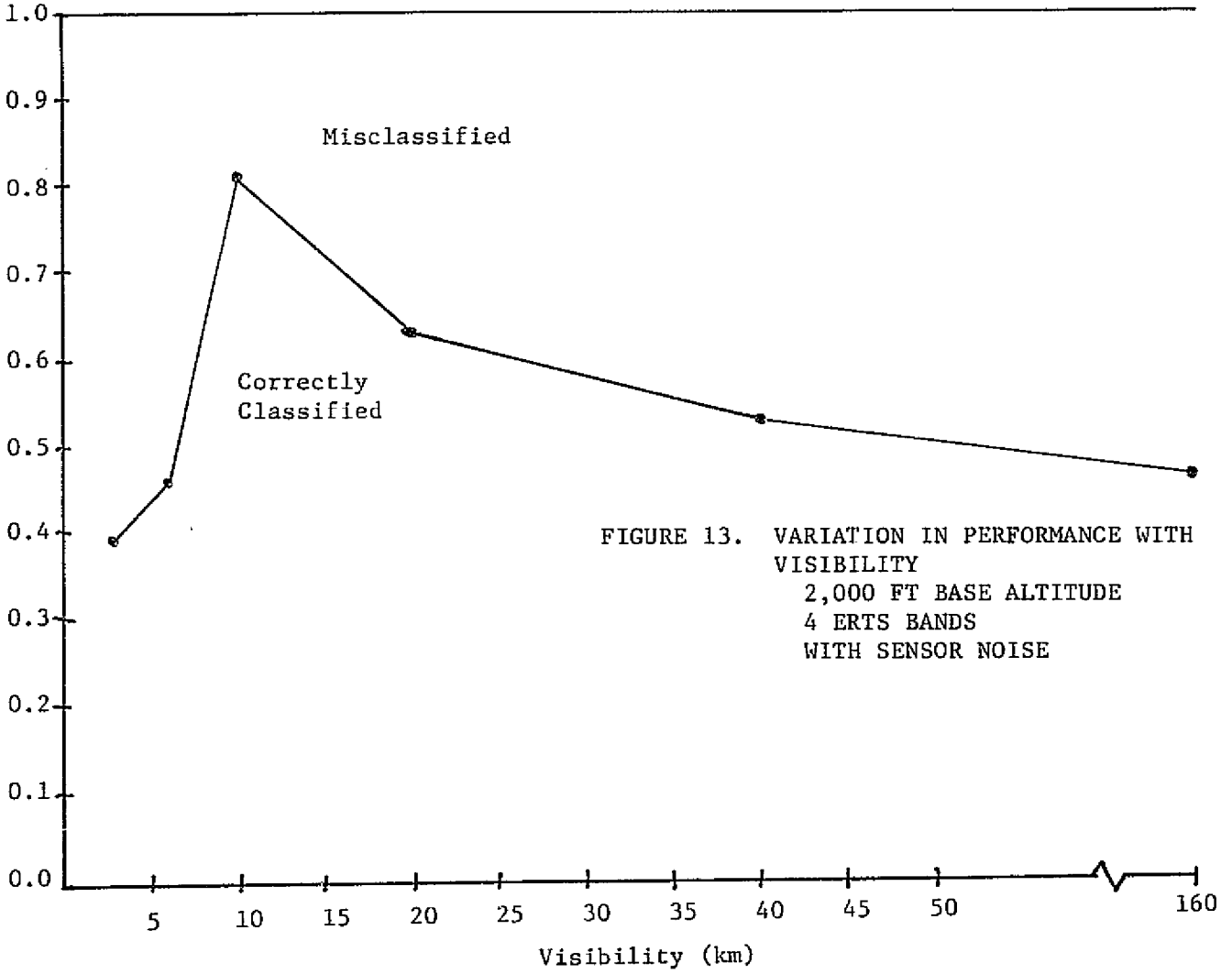

FIGURE 13. VARIATION IN PERFORMANCE WITH VISIBILITY
2,000 FT BASE ALTITUDE
4 ERTS BANDS
WITH SENSOR NOISE

Figures 14 and 15 show the variation in performance with four simulated ERTS bands as the altitude is varied from 2,000 to 6,000 ft at a visibility of 10km. These curves are comparable to Figures 8 and 9 for the four optimum channels. Again, the qualitative behavior of average probability of correct classification as conditions are varied away from the training condition is similar for ERTS and four optimum channel cases. For the four optimum band case, an altitude variation from 2,000 to 2,390 ft caused a 5% decrease in performance. An altitude change from 2,000 to 2,760 ft would cause a 5% decrease in the performance using the four ERTS bands. One reason why a greater altitude variations are possible with ERTS than with the four optimum bands might be that the ERTS bands are confined to the green, red, and near-infrared portion of the spectrum, while the four optimum bands include one band in the blue-green where path radiance is a large fraction of the observed signal and where variations with altitude are large. Further, most vegetation has low reflectance in the blue-green as a consequence of chlorophyll absorption. Hence path radiance changes will lead to large changes in signature mean values for vegetation classes.

Figures 16 and 17 show the variation in performance as altitude is varied from 6,000 to 14,000 ft at a visibility of 40km. Compare these figures with Figures 10 and 11 for the four optimum bands. As with the four optimum band case less than 5% performance degradation is observed over most of the range. Again the performance increases, then decreases as we increase altitude from 8,000 to 14,000 ft. The reason for this behavior was discussed in Section 2.5.1.

For the noise-free case for four optimum channels the performance decreased smoothly as elevation was increased from 8,000 to 14,000 ft. This behavior is noticed to a much smaller degree in the ERTS data. Again the difference is probably caused by the blue-green band being one of the four optimum bands, but not one of the four bands used to

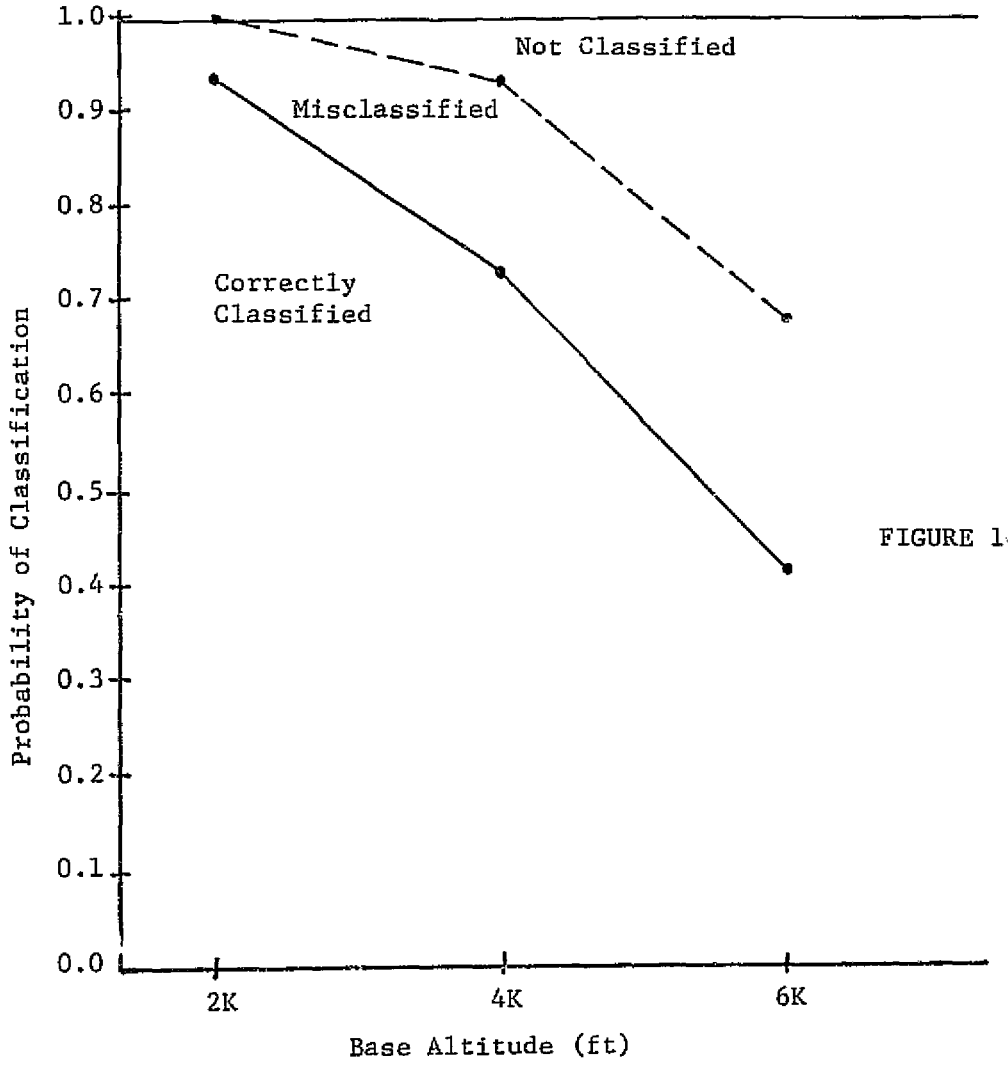

FIGURE 14. VARIATION IN CLASSIFIER PERFORMANCE WITH BASE ALTITUDE
10km VISIBILITY
4 ERTS BANDS
NOISE FREE

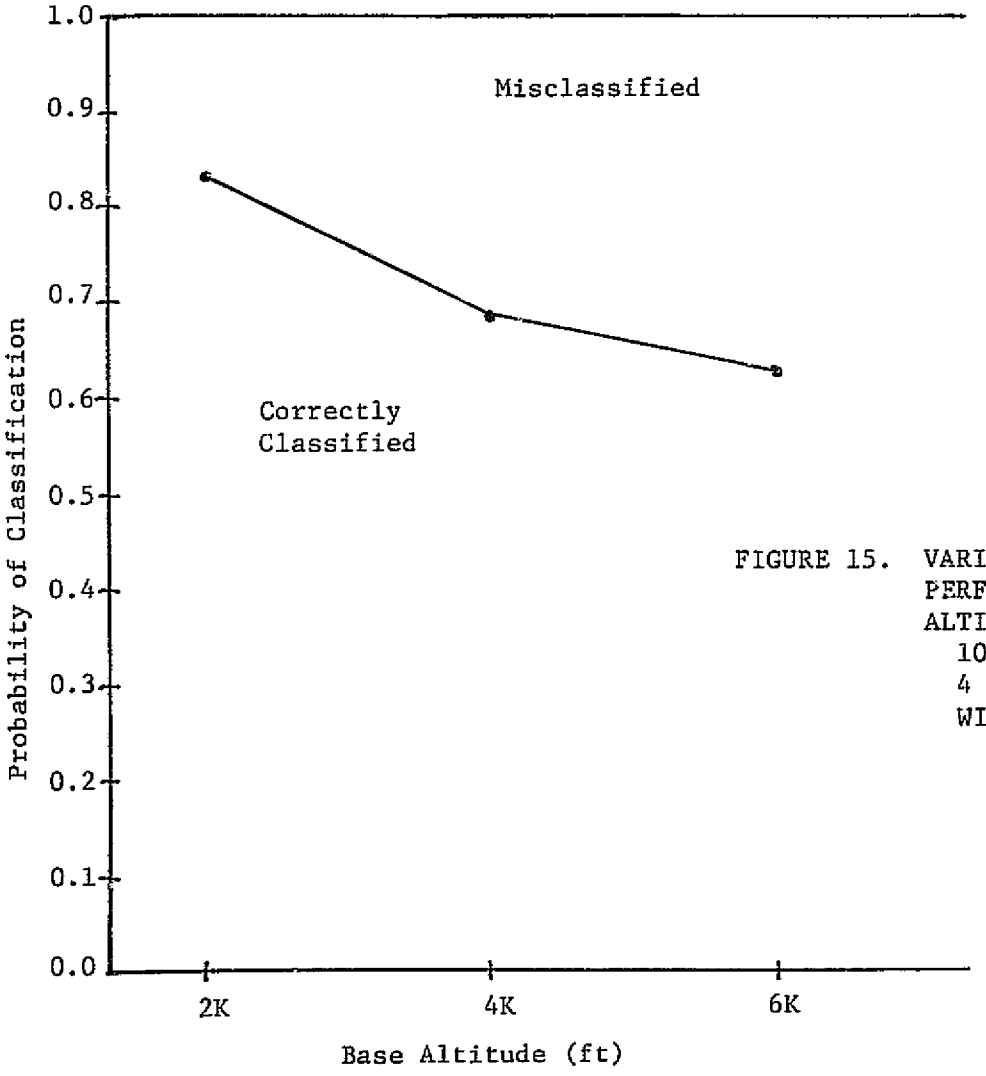

FIGURE 15. VARIATION IN CLASSIFIER PERFORMANCE WITH BASE ALTITUDE
10km VISIBILITY
4 ERTS BANDS
WITH SENSOR NOISE

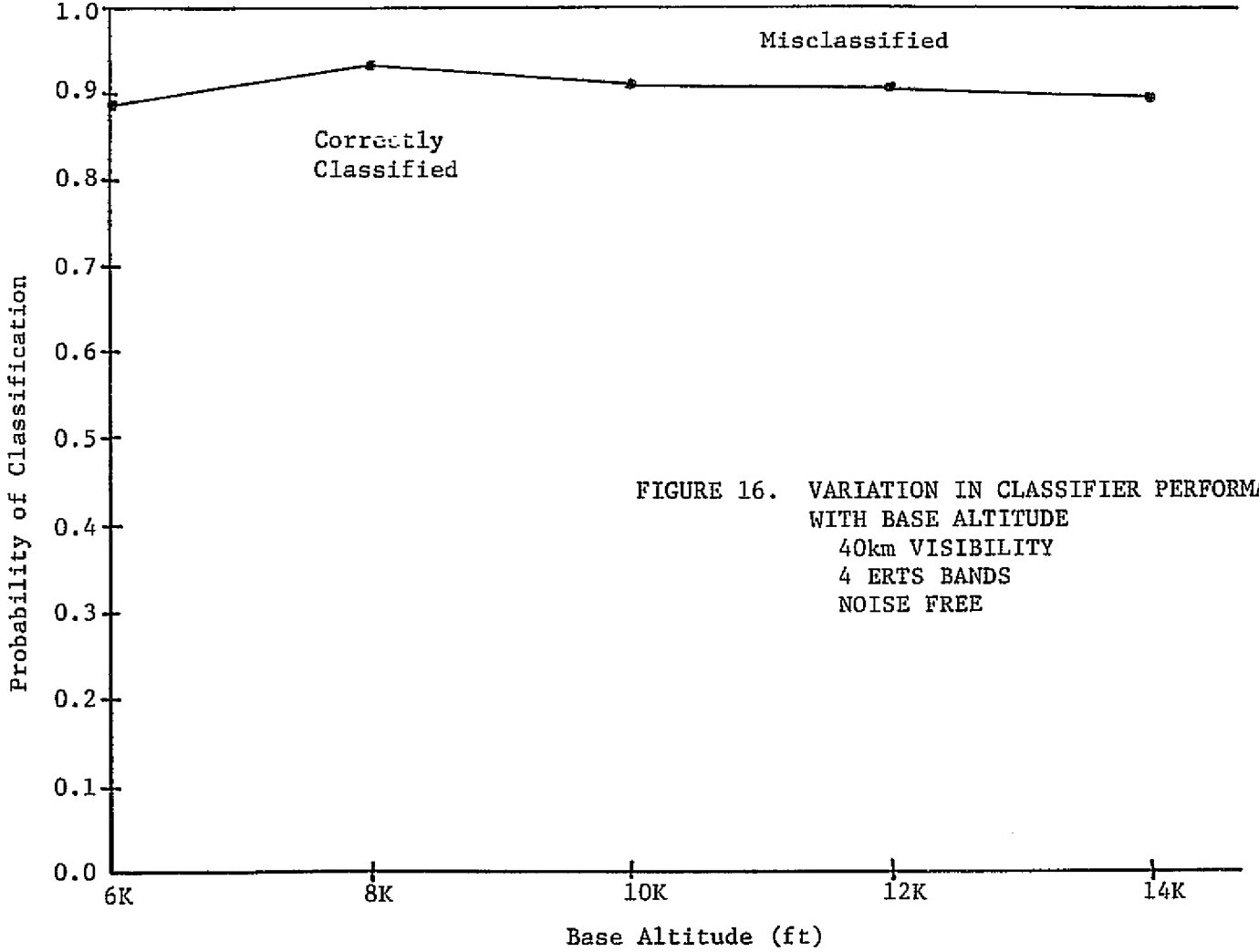

FIGURE 16. VARIATION IN CLASSIFIER PERFORMANCE WITH BASE ALTITUDE
40km VISIBILITY
4 ERTS BANDS
NOISE FREE

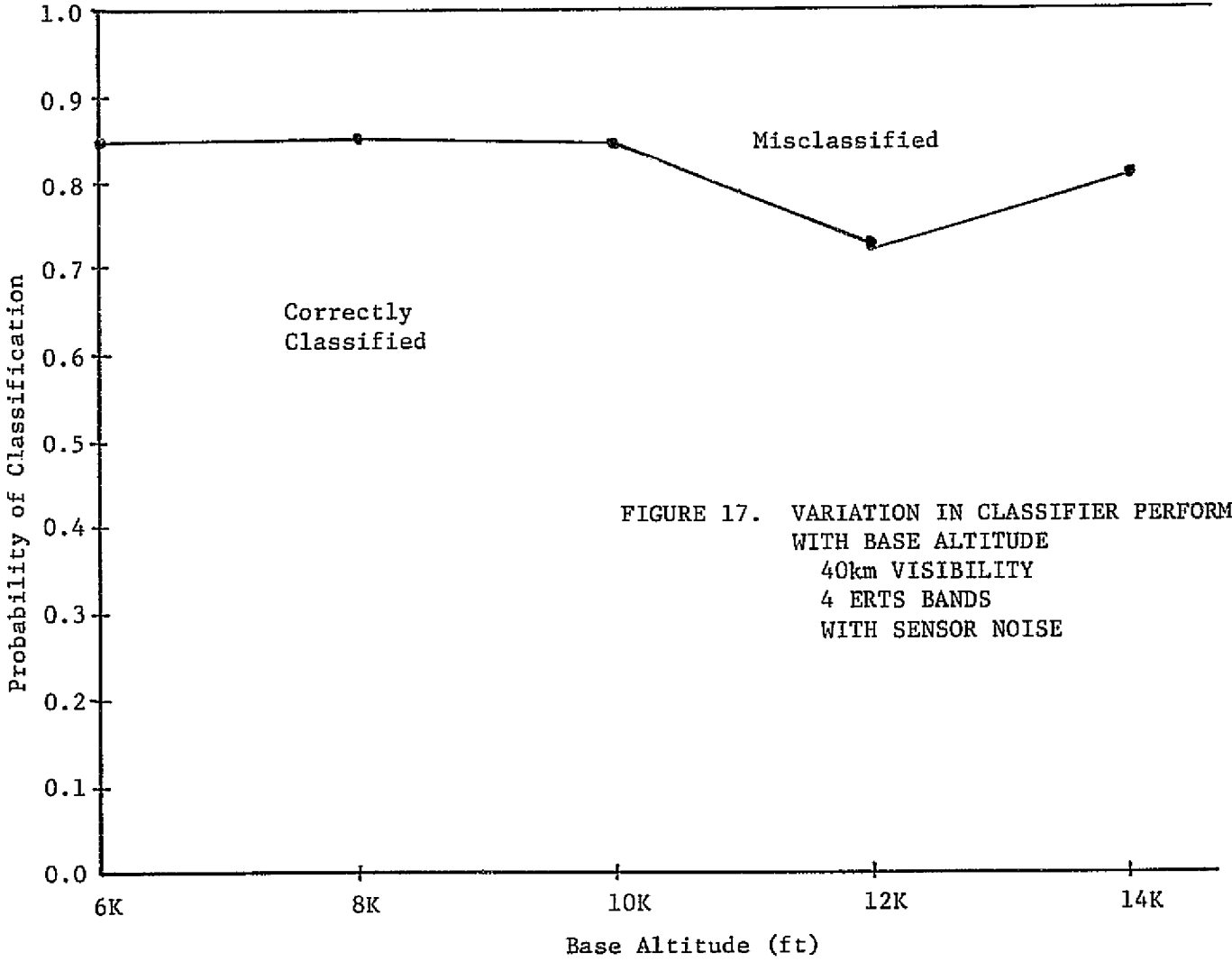

FIGURE 17. VARIATION IN CLASSIFIER PERFORMANCE WITH BASE ALTITUDE
40km VISIBILITY
4 ERTS BANDS
WITH SENSOR NOISE

simulate ERTS. For this band changes in atmospheric effects (primarily path radiance for dark vegetation targets) will be relatively larger for a given terrain elevation or visibility change than for the green or red bands of ERTS.

Comparing the simulated performance of the four simulated ERTS bands with that of the four optimum bands, the ERTS bands show better performance at the training condition than the four optimum bands primarily because of lower noise levels simulated for the ERTS sensor. Performance degradations with visibility changes are similar for the two four band sets. Changes with elevation differences are slightly smaller for ERTS bands than for the four optimum bands, the latter set with a blue-green band.

2.5.3 SEVEN OPTIMUM BAND RESULTS

Figures 18 and 19 show the classifier performance in noise-free and noisy cases for seven optimum channels. In this case, the seven channels were 0.48 - 0.52, 0.50 - 0.54, 0.55 - 0.60, 0.62 - 0.70, 0.67 - 0.94, 1.0 - 1.4, and 1.5 - 1.8 μm, and the noise simulated was for the S-192 sensor. Comparing the performance of the seven channels with that of the four optimum or four ERTS simulated channels, the performance at the training condition is slightly better (0.881 average probability of correct classification versus 0.719 and 0.817 respectively for the noisy cases and 0.988 average probability of correct classification versus 0.942 and 0.938 respectively for the noise-free cases). For the noise-free case, the degradation in performance as conditions are varied from the training condition is more drastic for the seven channel case than for either of the four channel cases. This makes sense intuitively because the decision regions associated with each signature are proportionally larger for seven channels than for four channels, but the additional three channels (.50 - .54, .67 - .94, and 1.0 - 1.4 μm) have larger variations in atmospheric effects with

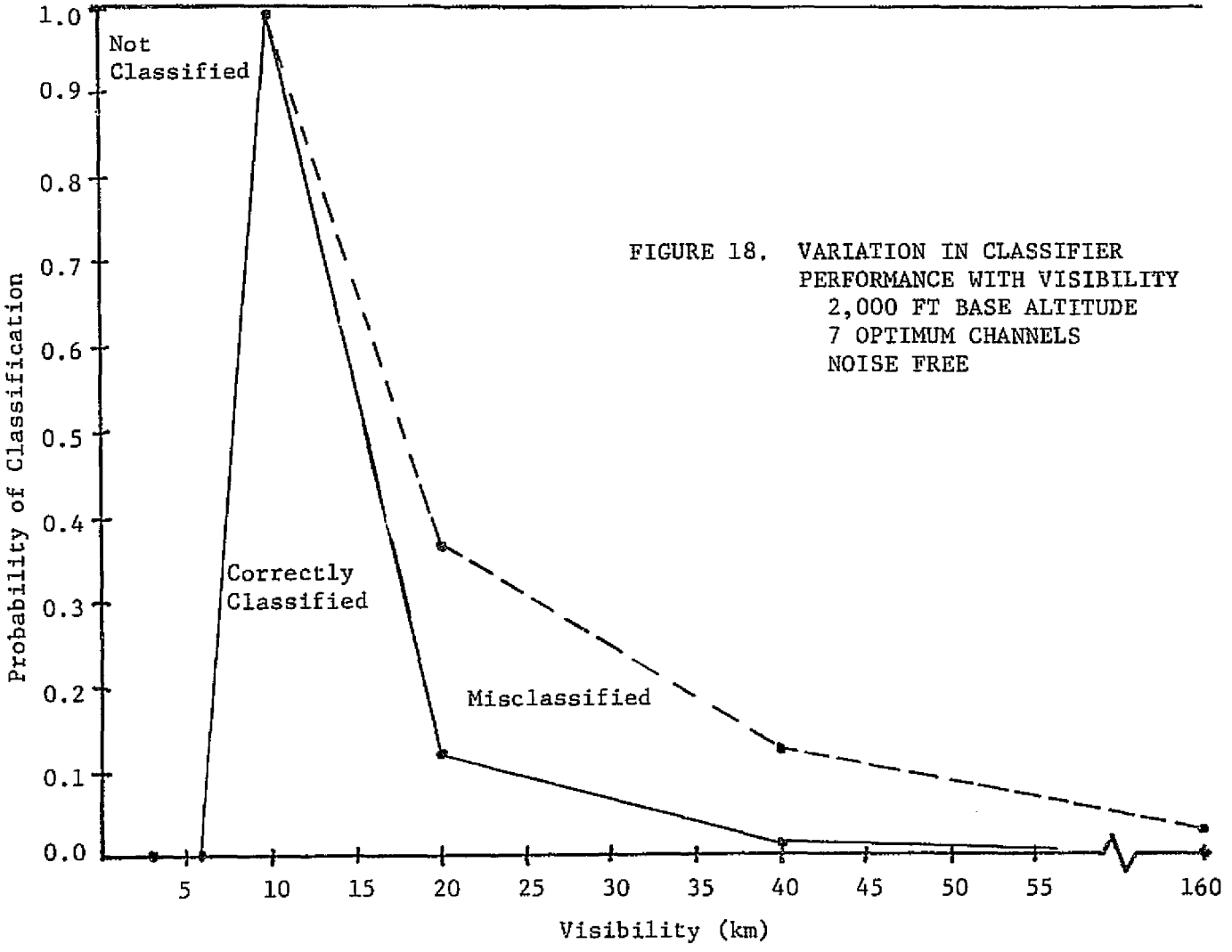

FIGURE 18. VARIATION IN CLASSIFIER PERFORMANCE WITH VISIBILITY
2,000 FT BASE ALTITUDE
7 OPTIMUM CHANNELS
NOISE FREE

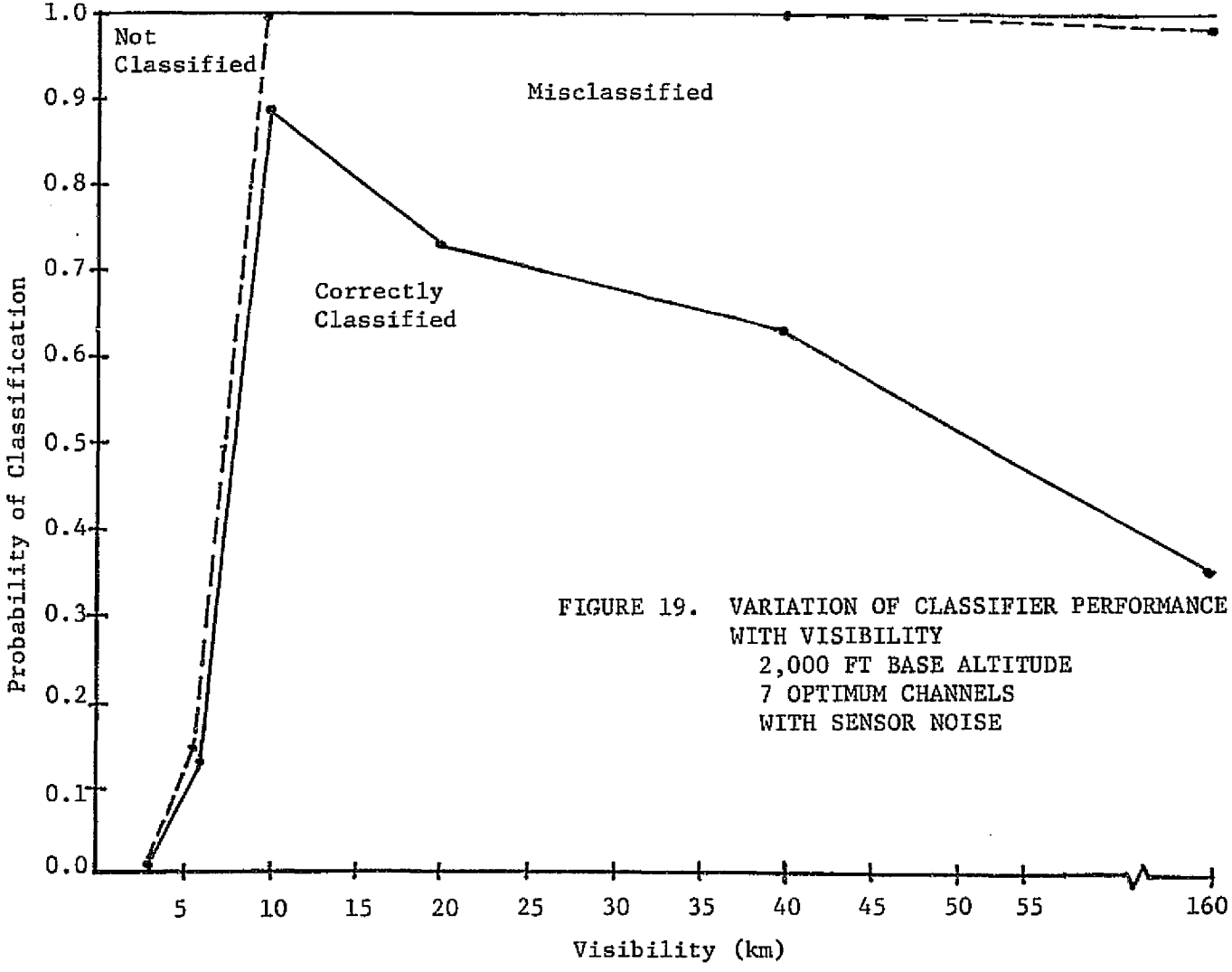

FIGURE 19. VARIATION OF CLASSIFIER PERFORMANCE WITH VISIBILITY
2,000 FT BASE ALTITUDE
7 OPTIMUM CHANNELS
WITH SENSOR NOISE

changing visibility than the optimum four. Hence a given visibility change will induce a greater change in performance for seven channels than for four.

For the noisy case, the degradation in performance as visibility decreases is also more severe for the seven channel case than for either of the four channel cases. But as visibility improves from the training condition of 10km, the seven channel results are less drastically affected than the four optimum channel results, until we reach the limiting case of 160km visibility.

As we saw with the four channel results, the major effect in the noise-free case is for correct classification probability to decrease and the not classified category to increase. For the noisy case, the probability of correct classification decreases and the misclassification increases.

If we accept a 5% decrease in classifier performance, then the range of visibilities over which we can operate with the seven optimum channels is 9.8km to 10.58km with the noise-free data and 9.74km to 13.3km for the case with sensor noise included. These ranges are narrower than for the 4 optimum or the 4 ERTS channels. This implies that the performance is more sensitive to atmospheric visibility variations when seven channels are used than when four channels are used.

A more realistic comparison of performance between the three cases is to specify a certain level of performance of all classifiers and then calculate the range of conditions over which the classifiers can deliver that performance. If we somewhat arbitrarily select 65% accuracy on the training sets, then the range of visibilities over which we can obtain this performance is as shown in Table 5.

Table 5 contains much interesting information about the variation in classifier performance with visibility. First, for the noise-free case, note that the four ERTS bands have the widest range of applicability.

TABLE 5

RANGE OF VISIBILITIES OVER WHICH
65% TRAINING SET ACCURACY CAN BE ACHIEVED
(Training at 10km Visibility)
(2000 ft base elevation)

Case	Upper Visibility Limit (km)	Lower Visibility Limit (km)
4 OPT (noise free)	16.9	8.74
4 ERTS (noise free)	19.8	8.44
7 OPT (noise free)	13.9	8.63
4 OPT (sensor noise)	14.6	8.79
4 ERTS (sensor noise)	19.02	8.13
7 OPT (sensor noise)	36.4	8.76

This occurs because the performance at the training condition is good and the performance does not degrade too rapidly with changes in visibility because the four bands used to simulate ERTS are far enough into the red to avoid most of the major changes in atmospheric effects with visibility, which occur in the blue. By comparison, the range of the four optimum bands is smaller than the four ERTS bands for the noise-free case. Better performance at the training condition is offset by greater variation in performance away from the training condition because the four optimum bands contain a blue-green band more sensitive to atmospheric effects than the ERTS bands. Thus while the four bands are optimum for separating the classes at the training condition, they may not necessarily be optimum for signature extension over visibility changes. The seven optimum channel noise-free results show greater sensitivity to atmospheric visibility changes than the four optimum channel results. Here too, the increased performance at the training condition is offset by greater sensitivity to atmospheric effects which change with visibility. Thus the number of channels used for classification under conditions where signatures must be extended over visibility variations must be selected with signature extendability, as well as classifier performance on the training sets, in mind.

Comparing the cases where sensor noise was also simulated, the four ERTS bands still have a larger range of permitted visibility variations for a performance of 65% than the four optimum bands. The lower visibility limit is slightly lower for the noisy ERTS case than for the noise-free case because the performance under noisy conditions falls off more slowly with decreasing visibility than under noise-free conditions. The four optimum band case has the most restricted operating range under conditions where S-192 sensor noise was simulated. The seven optimum band case has the widest range of operation under these noisy conditions, mainly because of the slow degradation of performance with increasing visibility.

Figures 20 and 21 show the variation of classifier performance for seven optimum bands, with and without sensor noise respectively, as base elevation is varied from 2,000 - 6,000 ft for a visibility of 10km. For both cases, the performance decreases as we move away from the 2,000 ft training altitude. The effect is more drastic for the noise-free case than for the noisy case. As we move away from the training altitude, the major effect in the noise-free case is a reduction of correct classification and an increase in not classified. Under S-192 noise conditions a more gradual decrease in correct classification occurs and an increase in misclassified. Similar effects were noted when visibility was varied away from the training conditions.

Table 6 summarizes the range of altitudes over which 65% or better average correct classification can be achieved for the various cases. The same qualitative comments apply to this table as to the previous table where visibility ranges were tabulated. For the noise-free case, the four ERTS bands show the largest altitude range for "acceptable" performance. The four optimum bands show a reduced altitude range because of the blue-green band being one of the four optimum. The seven band case shows the smallest altitude range. For the noisy case, the seven band case shows the largest altitude range and the four optimum band case the least altitude range. The four ERTS band case is intermediate.

Figures 22 and 23 show the variation in classifier performance with base altitude changes at 40km visibility for seven optimum bands for noise free and noisy cases respectively. As with the two four channel cases there is a decrease in correct classification and an increase in misclassification as we move away from the 8,000 ft training altitude. But for the seven channel case the degradation in performance is more drastic for the noise-free case than for the noisy case, in contrast to the four channel results.

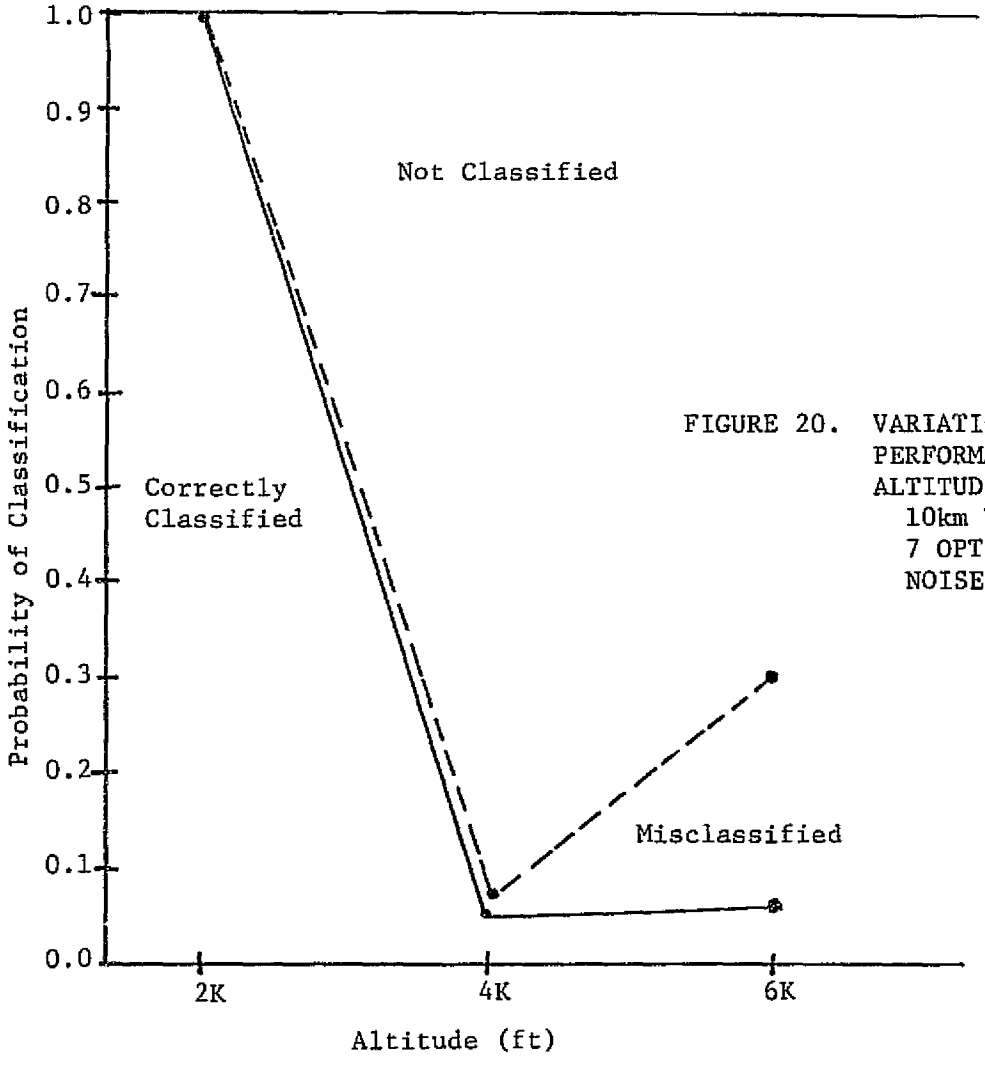

FIGURE 20. VARIATION IN CLASSIFIER PERFORMANCE WITH BASE ALTITUDE VARIATION
10km VISIBILITY
7 OPTIMUM CHANNELS
NOISE FREE

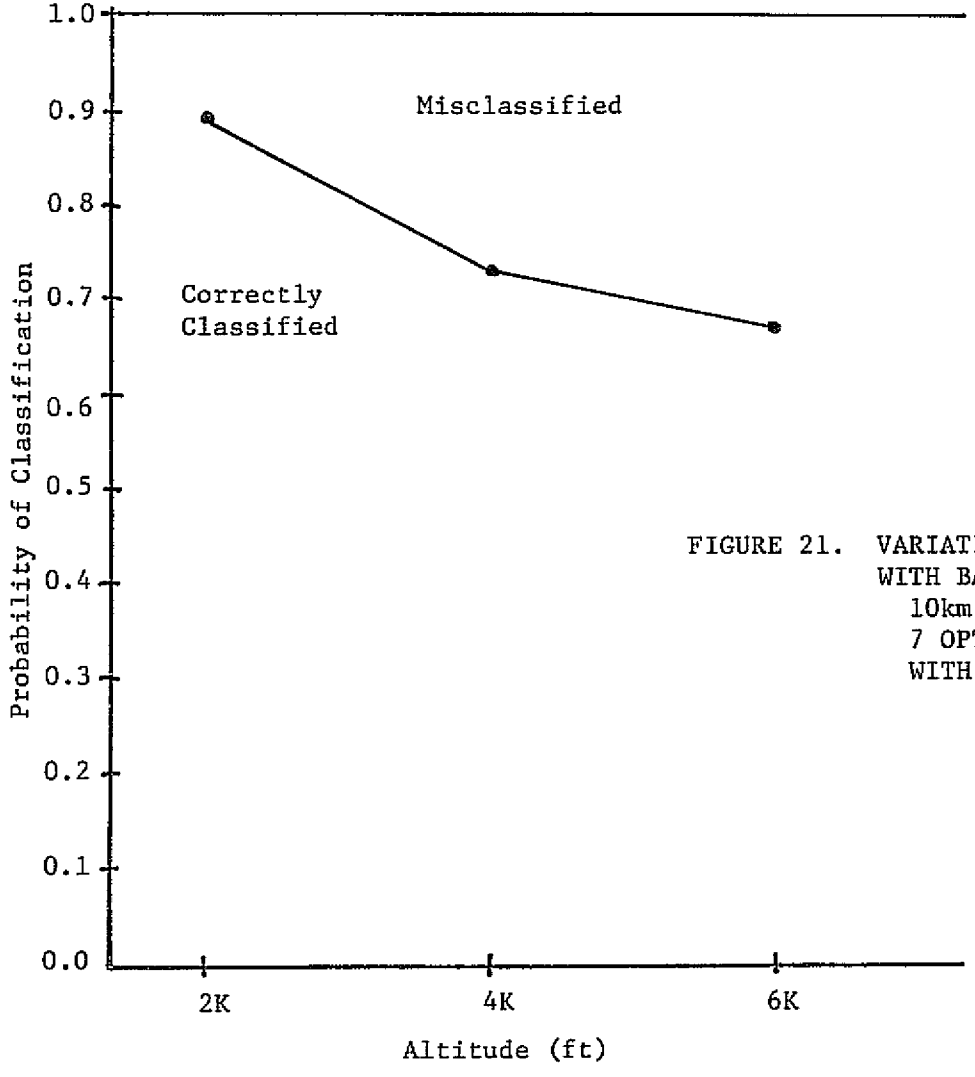

FIGURE 21. VARIATION OF CLASSIFIER PERFORMANCE WITH BASE ALTITUDE VARIATION
10km VISIBILITY
7 OPTIMUM CHANNELS
WITH SENSOR NOISE

TABLE 6

RANGE OF BASE ALTITUDES OVER WHICH
65% TRAINING SET ACCURACY CAN BE ACHIEVED
(10km Visibility, Training at 2,000 ft)

Case	Upper Altitude Limit (kft)	Lower Altitude Limit (kft)
4 OPT (noise free)	3.08	2.0
4 ERTS (noise free)	4.52	2.0
7 OPT (noise free)	2.72	2.0
4 OPT (sensor noise)	2.67	2.0
4 ERTS (sensor noise)	5.21	2.0
7 OPT (sensor noise)	6.0*	2.0

*performance not degraded to 65% at 6.0kft

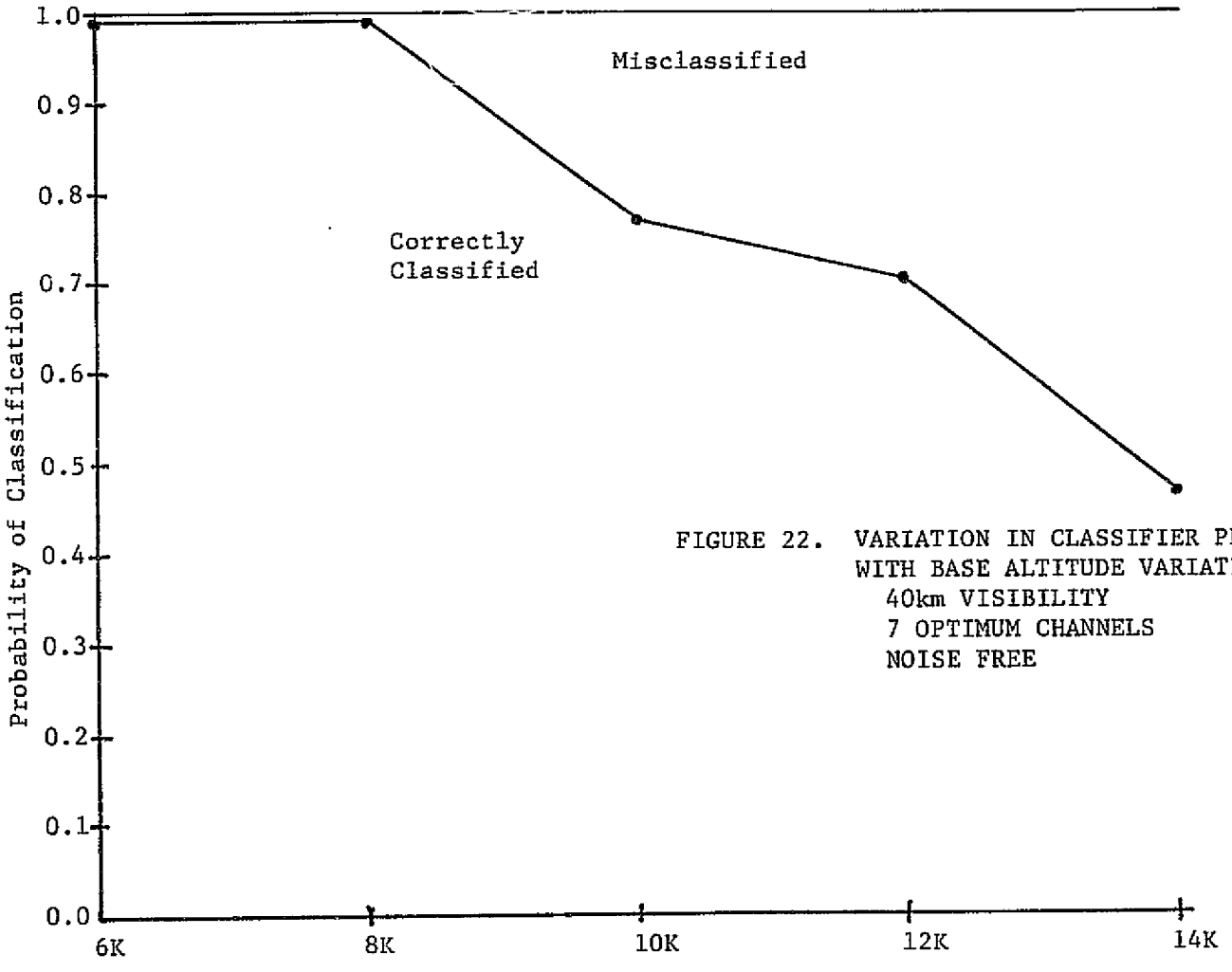

FIGURE 22. VARIATION IN CLASSIFIER PERFORMANCE WITH BASE ALTITUDE VARIATION
40km VISIBILITY
7 OPTIMUM CHANNELS
NOISE FREE

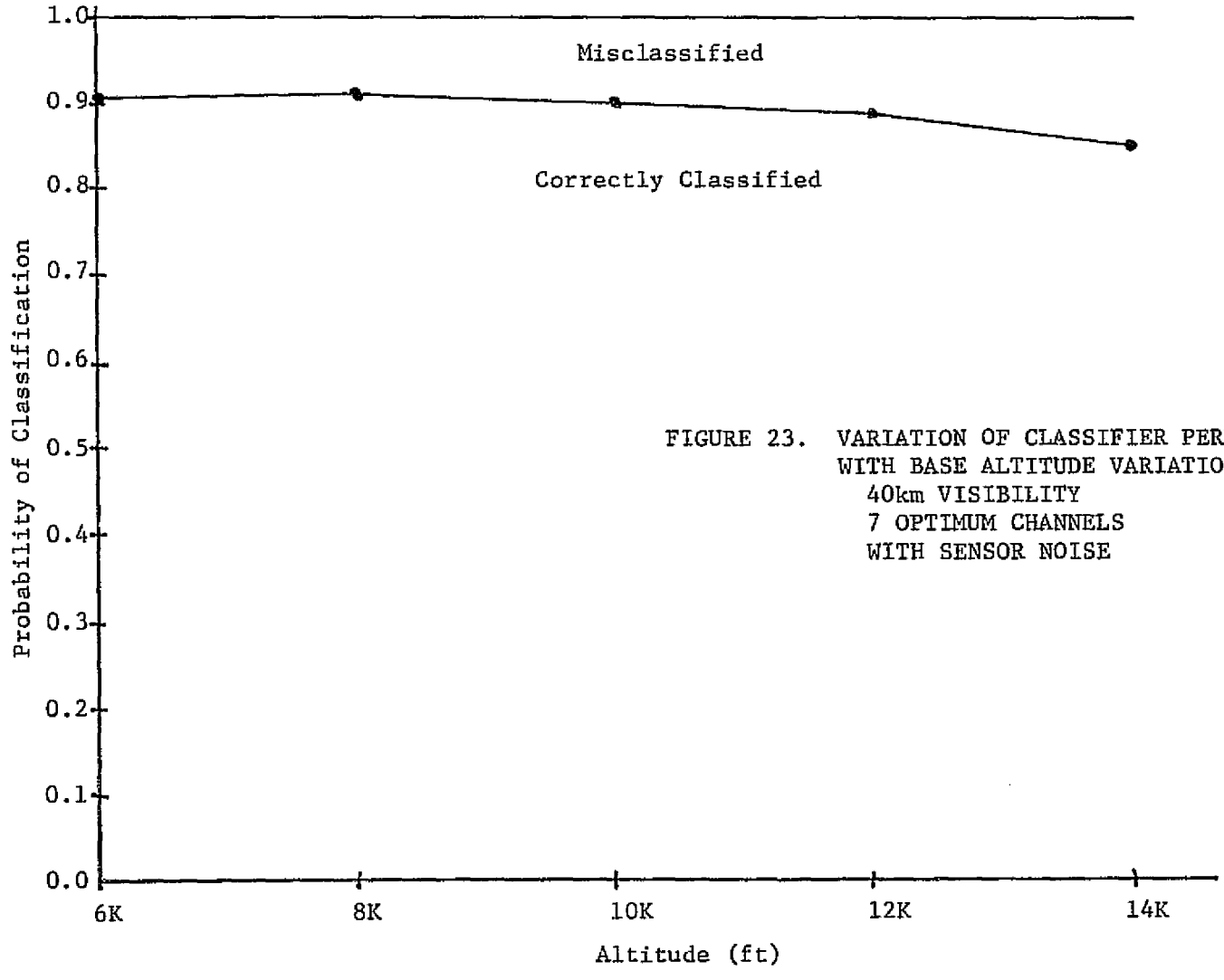

FIGURE 23. VARIATION OF CLASSIFIER PERFORMANCE WITH BASE ALTITUDE VARIATION
40km VISIBILITY
7 OPTIMUM CHANNELS
WITH SENSOR NOISE

Using the 65% or greater correct classification criterion, acceptable performance is obtained over the entire range of altitudes for all cases except the seven channel noisy case, where the specified performance can be obtained only from 6,000 to 12,000 ft.

2.5.4 MODEL VERIFICATION WITH ACTUAL SKYLAB PROCESSED RESULTS

In an effort to verify that the model results (particularly those results where sensor noise was simulated) were accurate, we processed actual S-192 data collected over the Michigan Test Site on 5 August 1973. The details of processing are discussed in Sections 2.3 and 2.6. The training sets selected from the S-192 data were the same as those selected from the aircraft data from which the reflectance signatures were obtained. Training and test set performance were evaluated. These results are more fully discussed in Section 2.6. However, Table 7 presents a comparison of training set accuracies from the simulated S-192 data and the actual S-192 data. The 2,000 ft base elevation and 10km visibility conditions are reasonably close approximations to the actual conditions at the Michigan Test Site during the Skylab overpass [3]. As can be seen from Table 7, the agreement between the two results is good, particularly when the 90% confidence intervals of the estimate from the actual data are considered. These confidence intervals are important because of the relatively small number of points (435) used for the evaluation of actual S-192 data. All simulated results fall within the 90% confidence intervals of the actual results, except corn, soybeans, and the average. Differences may be attributed to the slight difference in the actual and simulated spectral bandwidths, the slight difference between the simulated conditions and the actual conditions, and to minor variations in actual S-192 sensor noise from that tabulated in reference 4. The fact that signatures are not really gaussian, but were assumed so for the simulation is also a factor which must be considered. But on the whole, the agreement between simulated and actual seven optimum band S-192 results is good, lending credibility to the conclusions to be drawn from the simulation study.

TABLE 7

COMPARISON OF SIMULATED S-192 AND
ACTUAL S-192 TRAINING SET CLASSIFICATION
ACCURACY RESULTS FOR 2,000 ft BASE
ALTITUDE AND 10km VISIBILITY

Class	Simulated Accuracy	S-192 Accuracy*
Corn	83.4	73.8 ± 8.1
Woods	91.1	78.6 ± 3.7
Soil	90.7	90.5 ± 11.3
Soybeans	86.0	68.1 ± 17.0
Other	89.6	90.0 ± 7.2
Average	88.2	80.2 ± 4.8

*mean value ± 90% confidence interval

2.5.5 CONCLUSIONS FROM THE SIMULATION STUDY

Conclusions reached from the simulation study are reported in this section. When reading these conclusions, the reader should be aware that this is but one study, using one set of data of one agricultural scene. The conclusions drawn are supported by the results of the experiment. Generalization to a broader agricultural mapping problem should be done with care, and with due regard for other studies relating to this general problem (e.g., reference 6).

Under training conditions, and noise-free conditions, the seven optimum channels perform better than the four optimum and four simulated ERTS bands (0.988 versus 0.942 and 0.938 average probability of correct classification). But the seven optimum channel results are more sensitive to changes in atmospheric visibility (Table 5) or base elevation (Table 6). When S-192 or ERTS sensor noise is simulated this behavior is not as dramatic.

Classification using the four narrow aircraft data bands to simulate ERTS bands is less affected, in either noisy or noise-free state, by changes in atmospheric or base elevation conditions than classification using the four optimum bands. This is probably because a blue-green band is one of the four optimum bands, and variations in atmospheric effects in this band are larger than for the simulated ERTS bands.

The performance using narrow wavelength bands to simulate ERTS, and four optimum channels, are nearly the same under noise-free conditions (0.942 versus 0.938 average probability of correct classification). Under conditions of sensor noise, the four simulated ERTS bands show better performance than the four optimum bands, probably because the noise levels from the ERTS sensor are generally lower than from the S-192 sensor.

The seven channel results with sensor noise agree well with actual performance on the same fields from the S-192 processing. Small

differences in performance may be attributed to slight mismatch of simulation study bands and actual S-192 bands, to slight differences between simulated and actual atmospheric conditions, and to lack of strictly gaussian training set statistics. The good agreement between simulated and actual results verifies that the noise conditions used for S-192 were representative of the noise in the data.

The implications for use of ERTS and S-192 like sensors for agricultural surveys relate to the range of atmospheric variability over which acceptable performance can be achieved. At atmospheric conditions equivalent to horizontal visibilities of about 10km, adequate performance (65% correct classification or better) can be obtained over atmospheric state variations corresponding to visibility variations of $\pm$ 3 - 4km. If greater variations are found, data preprocessing corrections will have to be made to assume adequate performance. Although training at other than 10km visibility conditions was not performed, it is expected that as the visibility improves, the range of visibilities over which adequate performance can be obtained will increase.

The implication for the use of future spacecraft sensors, with improved signal-to-noise ratio is contained in a comparison of noisy versus noise-free results. The noise-free results (as would be generated with a sensor with no noise) show better performance at the training condition but greater sensitivity to changes in atmospheric condition or base elevation than the noisy results. As better sensors are constructed, there should be more concern about selecting a set of bands and a number of bands to use for classification. The bands selected and the number of bands can only be partially specified by results of optimum channel studies and training set results generated under a limited set of atmospheric conditions. Due consideration must also be given to the range of atmospheric conditions over which surveys will operate. For example, in the present study, seven optimum channels

(noise-free) gave better performance at the training condition than four optimum channels, but the seven channel results were more sensitive to changes in atmospheric visibility than the four channel results. Which set would perform better in practice would depend on the user's definition of acceptable performance, but for 65% accuracy or better, the four channel results showed a wider range of visibilities than the seven channel results.

2.6 S-192 DATA HANDLING

The purpose of processing the S-192 data was to generate a recognition map comparable to the aircraft data recognition map and to evaluate its accuracy for comparison with the aircraft data and with the model calculations. The data used were SL-3 S-192 data collected over the Williamston, Michigan Test Site on 5 August 1973 at about 1100 EDT.

Referring to Figure 24, the first step in processing was to convert the S-192 data into 7094 computer format through the use of an IBM 360 conversion program. Then a reconnaissance graymap of the 1.5 - 1.8 μm band (every 10th line and point) was made to edit the area to that of the test site.

Next a 1 x 1 gray scale optimized map of the 1.55 - 1.75 μm band was prepared to select training sets, and the same training sets selected for aircraft data analysis were located. Then signatures were extracted for these fields from the S-192 data. As before, at least two samples of each of seven agricultural classes were selected, and the samples of each class combined to form the signature for that class.

A recognition map was prepared, using the optimum seven bands as selected from the analysis of aircraft data [6]. The bands used are shown in Table 8. When the recognition map had been prepared, its accuracy was evaluated on both the training set and the test set. The test set selected was different from the one used for the aircraft data

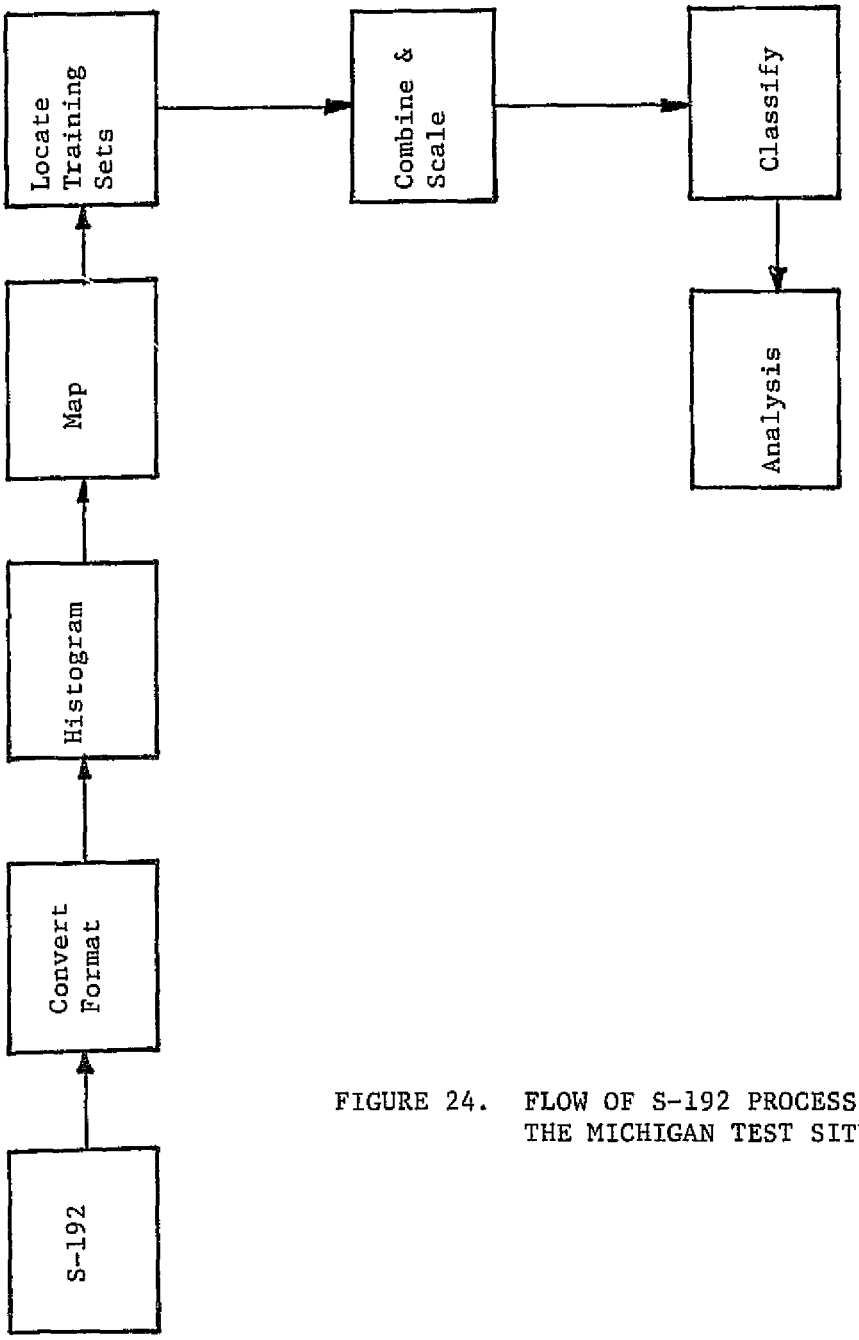

FIGURE 24. FLOW OF S-192 PROCESSING FOR THE MICHIGAN TEST SITE

TABLE 8

SEVEN OPTIMUM BANDS USED
FOR S-192 COMPUTER MAPPING OF
MICHIGAN AGRICULTURE

0.46 - 0.51 μm

0.52 - 0.56 μm

0.56 - 0.61 μm

0.62 - 0.67 μm

0.78 - 0.88 μm

0.98 - 1.08 μm

1.55 - 1.75 μm

evaluation [6] because it was impossible to find some of the small fields of the aircraft test set on the S-192 data.

2.6.1 TRAINING AND TEST SET LOCATION

Both training and test sets were difficult to find on the S-192 data graymap. This was caused by two factors — the resolution of the data and its radiometric quality, and the fact that conical scan data were used. (Scan line straightened data was originally requested, but was not used because other investigators had found mis-registration between the various channels of data in the scan-line straightened data [7].)

To accurately locate both training and test sets, we first prepared a grid overlay to the graymap showing all section lines. This grid was prepared by a two-step procedure. First, control points were located in both S-192 and aerial photographic data. Then section corners were measured from the aerial photography, using the same coordinate system as for the control points. A regression equation related the coordinates of the section corners in the photography to the line and point numbers on the S-192 data. The regression equation was developed from the control points.

The resultant section grid was only approximate, because of residual errors in the regression equations relating aerial photograph coordinates to S-192 data coordinates. Nevertheless, the grid was adequate for location of the training sets. A detailed comparison of the field pattern within a particular section grid and the pattern on the aerial photography allowed us to locate specific training and test fields which had been annotated on the photography.

2.6.2 EVALUATION OF MAP ACCURACY — TRAINING SETS

The evaluation of map accuracy was done on both training and test sets. For training set accuracy assessment, the actual classification within the training areas was counted. Initially, recognition as nine

separate categories were assessed. The recognition results were later aggregated to the five classes at interest in crop mapping surveys: corn, woods, soil, soybeans, and other. Some of the results of the analysis have already been presented in Table 7. Table 9 presents a confusion matrix of training set results showing not only percentage correct classification but how the various misclassifications are apportioned. In Table 9, the ground classes are shown across the top of the table, while the classifier classes are shown down the left hand side. For example, 73.8% of corn points were called corn by the classifier. The classifier called 10.6% of the corn woods, 10.0% soybeans, and 5.6% other. The numbers in parentheses show the standard deviation of the estimate of classification accuracy, computed assuming a binomial distribution.

Referring to Table 9, we see that corn is misclassified as woods, soybeans and other. The corn-woods misclassification, and corn-other misclassifications have been seen by other investigators using satellite and aircraft data [8,9]. The misclassification of corn as soybeans apparently occurs in sparsely vegetated areas of corn (drowned spots or field edges) more representative of soybeans than corn.

There is some confusion of bare soil with other, primarily stubble and pasture. There may be some vegetation growing in the bare soil fields used for training, and this would account for these misclassifications.

There is misclassification of woods as corn and soybeans. The woods corn misclassification has been mentioned before. Some sparse woods may be classified as soybeans.

The soybeans are confused with every other category except woods. This probably occurs because the soybeans had variable percentage cover of the ground at the time of overflight. Ordinarily this would not have occurred at this point in the growing season but 1973 was a very late year for crops as heavy spring rains delayed planting. Thus the soybeans were at a stage of development more typical of mid-July than

TABLE 9

CONFUSION MATRIX FOR AGRICULTURAL CLASSIFICATION
WITH SEVEN S-192 CHANNELS — MICHIGAN TEST SITE 8/5/73

Training Set Results

	Corn	Soil	Woods	Soybeans	Other
Corn	73.8 (3.27)	0	14.3	6.4	3.6
Soil	0	90.5 (4.52)	0	2.1	1.8
Woods	10.6	0	78.6 (5.48)	0	0
Soybeans	10.0	0	7.1	68.1 (6.8)	4.6
Other	5.6	9.5	0	21.3	90.0 (2.88)
Not Classified	0	0	0	2.1	0

Percentages of correct and mis-classification are shown. Numbers in parentheses are the standard deviations of the estimates.

early August. Very dense cover soybeans were misclassified as corn, "normal" cover areas were called soybeans, while sparse cover areas were called soil, other, and not classified. This kind of result was also seen in the test results. It is attributed to the delayed development of the soybean crop at the time of overflight in the summer of 1973.

The other class consisted of pastures, alfalfa and hay fields, and idle fields. While there were many misclassifications between the four signatures used to recognize this class, the recognition of the class as a whole was about 90%. The largest misclassification was as soybeans. The reason for this has been discussed above.

2.6.3 EVALUATION OF MAP ACCURACY — TEST SETS

Evaluation of accuracy on training sets frequently gives an artificially good estimate of the actual classifier performance. For this reason, test set evaluation of classifier performance was done. Table 10, shows the results of this evaluation for the four classes corn, woods, soil, and soybeans. The results are presented in the same format as Table 9. The results of Tables 9 and 10 are comparable — that is the accuracy results are within one standard deviation of each other — for all classes except soybeans. Comparing the soybeans results, we find larger misclassification as other and corn in the test set than in training set results. In view of the variability of the soybeans at this stage in the growing season, this result should be expected. Also, there are relatively few soybeans fields in the test area, and those fields are small. There was great difficulty in locating the soybeans test set fields.

On the whole, the results are as good as those being reports by other investigators [8]. They are probably representative of what can be done with S-192 data under these agricultural conditions. In a more normal year, we might expect improved performance on the soybeans category.

TABLE 10

CONFUSION MATRIX FOR AGRICULTURAL CLASSIFICATION
WITH SEVEN S-192 CHANNELS — MICHIGAN TEST SITE 8/5/73

Test Set Results

	Corn	Soil	Woods	Soybeans
Corn	71.1 (4.97)	0	11.6	14.3
Soil	0	85.7 (5.04)	0	0
Woods	22.9	0	81.4 (5.93)	0
Soybeans	0	7.0	4.8	50.0 (7.71)
Other	6.0	9.5	0	35.7
Not Classified	0	0	0	0

Percentages of correct and mis-classification are shown. Numbers in parentheses are the standard deviations of the estimates.

3

S-192 LAND RESOURCE MAPS OF CRIPPLE CREEK AREA

As a cooperative program with Dr. Harry Smedes of the U. S. Geological Survey, Denver, Colorado, and Mr. Jon Ranson, a Colorado State University graduate student, we prepared land resource maps of the Cripple Creek area of Colorado. The project was similar to one conducted with ERTS data [10] and resulted in a seven category computer-generated land resource map prepared using six optimum channels of S-192 data collected on 4 August 1973 at about 1719 hrs. GMT on the SL-3 mission.

3.1 TEST SITE DESCRIPTION

Figure 25 shows a portion of an S-190A red band (0.6 - 0.7 μm) frame with the test site outlined. Also shown is the outline of the ERTS project test site of [10]. S-192 data were collected over this site on various occasions, but the data from 4 August 1973 were selected for study because the vegetation categories were differentiable at that time, there was a minimum of snow cover, and the data were collected reasonably close to the time of the ERTS data previously processed. The area of Figure 25 covers a portion of south-central Colorado centered on the town of Cripple Creek. The area, about 20 x 25 miles in extent, extends from nearly Eleven Mile Canyon Reservoir on the northwest to beyond Colorado Springs on the east. The western half of the test site is mountainous terrain, while the eastern half is Great Plains. Pikes Peak is in the upper middle of the test site. Elevations within the test site vary from 5,000 ft for the Great Plains area to over 14,000 ft on Pikes Peak. Cripple Creek is about 10,000 ft elevation. The mountainous area consists of bare rock, coniferous forest over a variety of rock substrates, and grassland meadows. The Great Plains area consists of agriculture and rangeland. The rangeland

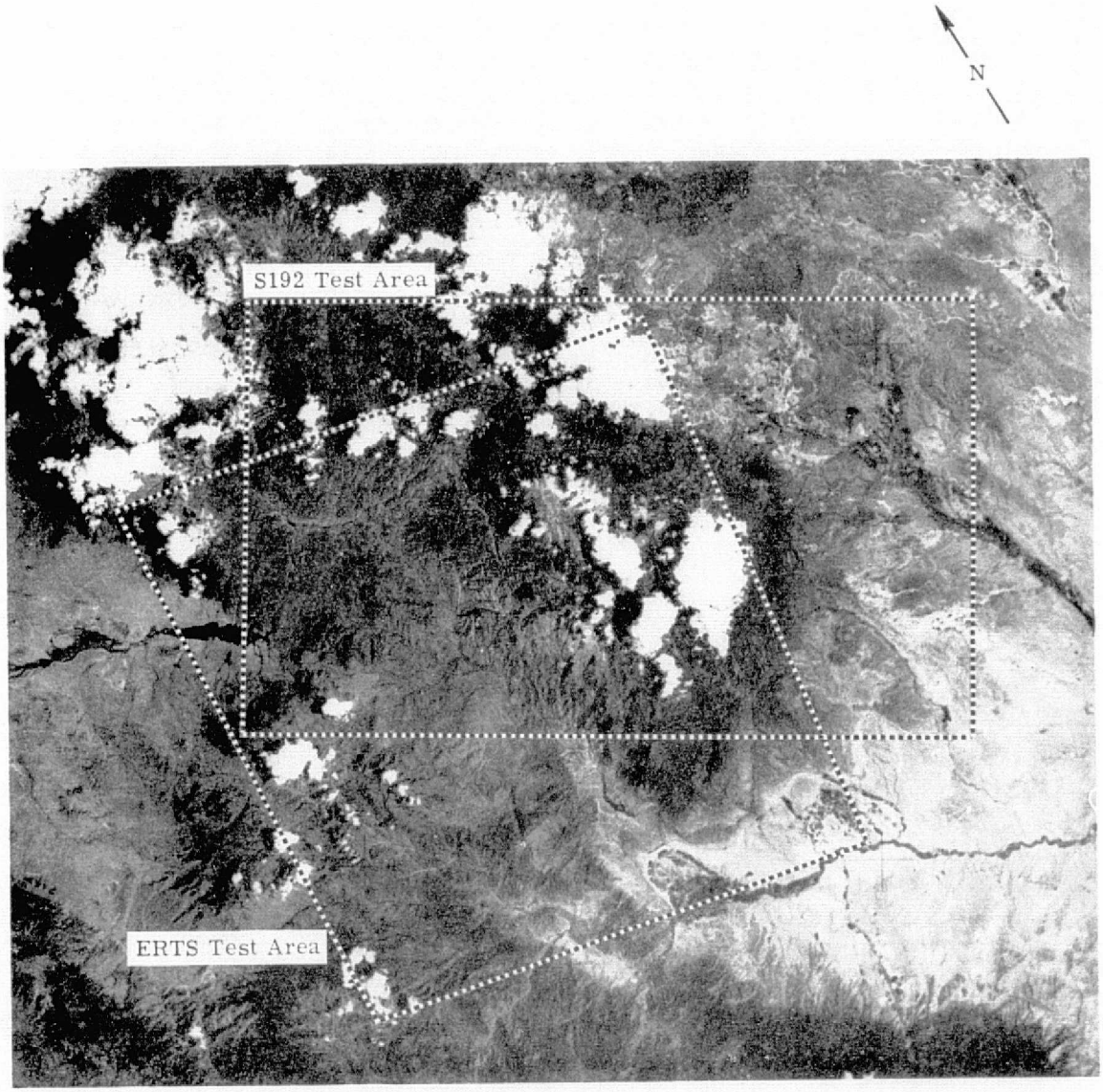

FIGURE 25. S190A RED BAND (0.6 - 0.7 μm) PHOTO OF TEST AREA FOR S192 MAPPING OF TERRAIN FEATURES, CRIPPLE CREEK, COLORADO, AUGUST 4, 1973.

has a sparse cover of grass. In between the mountainous terrain of the Rocky Mountains and the Great Plains, there are exposed a set of sedimentary rocks. These rocks were exposed when the Rocky Mountains were uplifted.

3.2 APPROACH

The approach to this land resource mapping task was to use computer-implemented pattern recognition processing of S-192 digital taped data. The flow of operations is summarized in Figure 26. We performed most of the computer processing at ERIM on an IBM 7094 computer. Dr. Smedes and Mr. Ranson assisted us by selecting the training sets and in providing guidance as to the final set of classes for mapping and display.

We began processing with scan-line straightened computer compatible tapes of S-192 data. The first step was the conversion of these data to a format compatible with our 7094 software package. The format conversion was done on an IBM 370/168 computer at the University of Michigan. Tapes in the ERIM standard format were then histogrammed to provide a quantiative measure of the dynamic range of data in all spectral channels. As with other S-192 digital tape data sets we have examined, we found the dynamic range in each channel to be a factor of 5 to 10 less than the maximum dynamic range of the tape.

We used histograms and the imagery of the scan line straightened data (also provided by NASA) to perform preliminary data quality assessment and to select a channel for mapping and for eventual selection of training sets. Examination of the imagery revealed that band 1 (0.41 - 0.48 μm) was so noisy as to be nearly useless. All other bands, including the thermal band (10.4 - 12.5 μm) showed adequate or good contrast. After careful examination of the imagery and histograms, band 11 (1.55 - 1.75 μm) was selected for mapping because it had the largest dynamic range of any of the channels, the imagery of that band

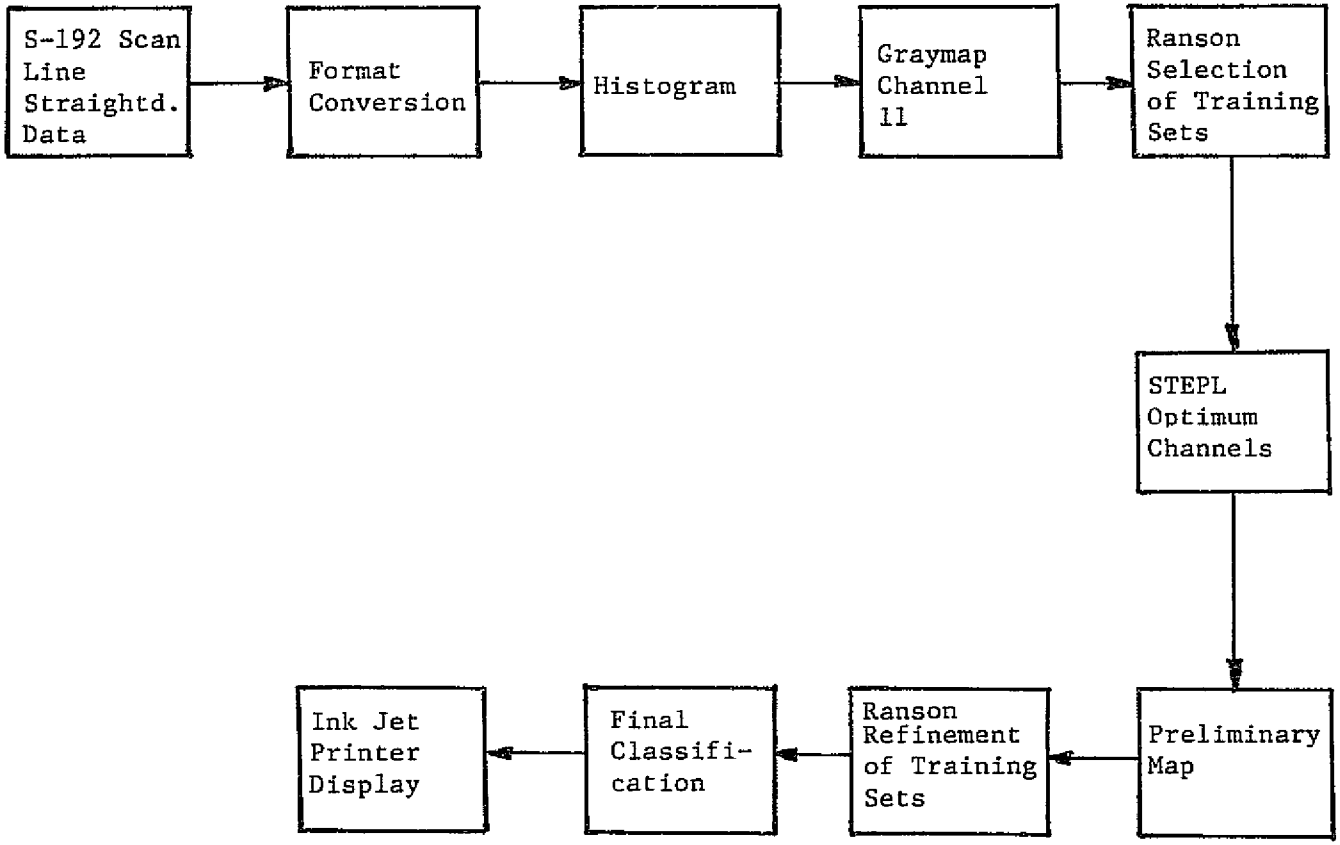

FIGURE 26. FLOW OF PROCESSING OPERATIONS — S-192 PROCESSING OF CRIPPLE CREEK DATA

showed good terrain contrasts, and the relative tones of vegetation, soil and rock, and water were similar to those in the red spectral region, permitting easy comparison of red band photography and the 1.55 - 1.75 μm computer map.

The 1.55 - 1.75 μm computer graymaps were sent to Dr. Smedes and Mr. Ranson for selection of training sets. They sometimes selected multiple areas to represent training sets for classes of materials they wished to discriminate in the data. Following the selection of training areas (see Table 11), and their designation to ERIM as sets of line and pixel numbers in the original S-192 data, spectral signatures were calculated. (A spectral signature is a description of the mean values, variances, and covariances of the signals in each spectral band for a particular material.) Copies of the signature information were sent to Dr. Smedes and Mr. Ranson who subsequently decided to combine the signatures of some classes whose signatures were not sufficiently different to permit reliable discrimination.

To assist them in deciding which of their original classes should be combined into composite classes, ERIM generated a set of pairwise probabilities of misclassification for each signature pair. The average pairwise probability of misclassification criterion was used to select six optimum bands for further mapping from the thirteen available S-192 bands [11]. A 7094 computer program, STEPL, was exercised for this selection. Two different runs of the program were made, one with all 22 terrain class signatures, and one with 14 signatures representing the bare rock and soil classes. Results of the channel selection for each of these cases are summarized in Table 12, with the consensus bands shown in Table 13. These results are further discussed in the next section. In selecting the bands for the consensus, where there was a choice, a band which appeared high in the ordering for separating rock types was selected, since the goal of the experiment was primarily to map rock types.

TABLE 11

TRAINING SETS SELECTED FOR CRIPPLE CREEK MAPPING

Designation	Brief Description
CCG	Cripple Creek Granite
DS	Dakota Sandstone
FOUNT	Fountain Formation
PHONGRAND	Phonolite - Granodiorite
PS	Pierre Shale
VOL	Volcanic Rocks
CCGC	Composite of Cripple Creek Granoite and Coniferous Forest
DSC	Composite of Dakota Sandstone and Coniferous Forest
GRANOC	Composite of Granodiorite and Coniferous Forest
PPG	Pikes Peak Granite
NS	Niobrara Shale
PPGC	Composite of Pikes Peak Granite and Coniferous Forest
VOLC	Composite of Volcanics and Coniferous Forest
CCGF	Dense Coniferous Forest over Cripple Creek Granite
GRANOF	Dense Coniferous Forest over Granodiorite
PPGF	Dense Coniferous Forest over Pikes Peak Granite
VOLF	Dense Coniferous Forest over Volcanics
CLOUD	Clouds
CLDS	Cloud Shadow
MEAD	Meadow (grass)
SNOW	Snow
WATER	Water

TABLE 12

ORDERING OF S-192 BANDS FOR TWO
CLASSIFICATION PROBLEMS — CRIPPLE CREEK

Order	General Classification	Rock Classification
1	1.55 - 1.75	0.56 - 0.61
2	0.78 - 0.88	1.55 - 1.75
3	1.09 - 1.19	0.68 - 0.76
4	2.05 - 2.35	1.09 - 1.19
5	10.4 - 12.5	2.05 - 2.35
6	0.62 - 0.67	0.62 - 0.67
7	0.68 - 0.76	10.4 - 12.5
8	0.56 - 0.61	0.78 - 0.88
9	.52 - .56	0.41 - 0.46
10	1.2 - 1.3	1.2 - 1.3
11	0.41 - 0.46	0.52 - 0.56
12	0.98 - 1.08	0.98 - 1.08
13	0.46 - 0.51	0.46 - 0.51

TABLE 13

CONSENSUS SIX BANDS FOR CRIPPLE CREEK
MAPPING FROM S-192 DATA

S-192 Channel	Wavelength (μm)
4	0.56 - 0.61
5	0.62 - 0.67
6	0.68 - 0.76
9	1.09 - 1.19
11	1.55 - 1.75
12	2.05 - 2.35

Following the selection of a consensus set of six bands for mapping, and the definition of a good set of classes for mapping (shown in Table 11), recognition maps of small test areas were prepared. This was done to permit a final assessment of the set of classes for mapping and to provide small test area information. After examination of the preliminary set of recognition maps by Mr. Ranson, a final set of classes, shown in Table 14, was defined and a final recognition map of the whole area was prepared.

Rather than display the recognition map using the conventional computer-printed map display, a more concise display format was sought. We had used the Mead Technology Labs ink jet printer to prepare concise display of ERTS recognition maps and considered it for the display of the final S-192 map. In the time between the preparation of the ERTS maps of reference 10 and the time we were ready to print our S-192 maps, a less expensive ink jet printer capability was developed as part of ERIM's MIDAS (Multivariate Interactive Digital Analysis System) [12]. We used MIDAS ink jet printer capability to generate the original of the color coded recognition map shown photographed in Figure 27. The cost of preparing this map was approximately $150.

3.3 DISCUSSION

The processing plan followed for the analysis of S-192 data was very similar to that for the analysis of ERTS data of the same area. Only the processing to identify optimum channels was added to the S-192 data processing. In this section, the results of the optimum channel analysis and the nature of the final classes of the recognition map of Figure 27 are discussed and compared with ERTS results.

3.3.1 OPTIMUM CHANNEL RESULTS

Any optimum channel results generated by channel selection programs and using training set statistics should be viewed with some caution. Both sensor data quality (signal-to-noise ratio) and the nature of the

TABLE 14

CLASSES OF THE FINAL CRIPPLE CREEK MAP

Undivided Sedimentary Rocks

Undivided Volcanic – Plutonic Rocks

Dense Forest

Sparse Forest

Meadow

Water and Cloud Shadow

Cloud and Snow

FIGURE 27. COLOR CODED INK JET PRINTER DISPLAY OF FINAL CRIPPLE CREEK LAND COVER MAP GENERATED FROM S192 DATA.

Legend

Green - Dense Forest

Violet - Sparse Forest

Yellow - Meadow

Brown - Sedimentary Rocks

Red - Volcanic Rocks

Black - Cloud Shadow and Water

White - Snow, Clouds and Not Classified

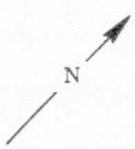

classes being mapped control which channels are selected. Any set of channels used for classification should be justified not only on the grounds of the channel selection program results, but also considering data quality and the nature of the reflectance signatures of the materials being discriminated. Considerations of data quality are particularly important in the case of S-192 data because of the obvious variation in signal-to-noise ratio from channel to channel. Thus, it may very well be that high signal-to-noise ratio, non-optimally placed spectral channels are selected before low signal-to-noise ratio optimally placed spectral channels because the low signal-to-noise obscures intrinsically larger signature separability in the optimally placed bands. This hypothesis must be examined before we can generalize from channel ordering results to say that a particular spectral band is a good one for a particular classification problem.

Table 15 lists the S-192 bands in order of decreasing signal-to-noise ratio. The data were obtained from reference 5. In the same table, the ordering of these bands for general classification and rock type mapping are presented. The conclusion drawn from Table 15 is that signal-to-noise ratio does not materially influence the order of selection of channels. For example, although channel 2 (0.46 - 0.51 μm) has the best noise equivalent reflectance, it is selected last for both general classification and for rock type mapping. Channel 11 (1.55 - 1.75 μm) has the ninth smallest noise equivalent reflectance but is selected first for general mapping and second for rock type mapping. Similarly channel 12 (2.05 - 2.35 μm), which has the largest noise equivalent reflectance of any of the reflective bands, is selected fourth best for general mapping and fifth best for rock type mapping.

Of the six bands selected for the classification, all can be justified on physical grounds. Referring to Table 13, the six bands selected bear marked similarity to the four ERTS bands plus two near infrared bands, and to early recommendations for the EOS Thematic

TABLE 15

ORDERING OF S-192 BANDS BY SIGNAL-TO-NOISE RATIO AND BY UTILITY IN TWO CLASSIFICATION PROBLEMS

		Mapping Utility	
Order	Sigan1-to-Noise	General	Rock
1	2	11	4
2	3	7	11
3	6	9	6
4	8	12	9
5	1	13	12
6	4	5	5
7	7	6	13
8	9	4	7
9	11	3	1
10	10	10	10
11	5	1	3
12	12	8	8
13	(13)	2	2

Mapper [6]. The bands of Table 13 are not listed in order of selection, but by increasing wavelength.

The 0.56 - 0.61 μm band is useful for vegetation assessment because it is close to the green peak (actually on the long wavelength side of the peak) of reflectance caused by lack of chlorophyll absorption. This band is also useful in discriminating rock types containing ferric iron because of the absorption by ferric iron in the yellow-green portion of the spectrum.

The 0.62 - 0.67 μm band is very useful in discriminating vegetation types (because it is placed near the red chlorophyll absorption dip) and is also useful in discriminating ferric iron containing rocks (when used with the 0.56 - 0.61 μm band) because of the lack of ferric iron absorption in the 0.62 - 0.67 μm region.

The 0.68 - 0.76 μm band may be useful in discriminating vegetation types. The band is located near the "shoulder" of the vegetation reflectance curve, where the vegetation reflectance rises steeply. Changes in the position or height of the shoulder would be reflected as changes in the reflectance in this band. The selection of this band third for rock type mapping cannot be justified by any particular spectral features in the spectra of the rocks in the test site.

The 1.09 - 1.19 μm band (or a band with similar response) has been found optimum for vegetation mapping in nearly every study addressing optimum bands. This band was also selected third for rock type discrimination, probably because the rock type training sets contained some vegetation as well as rock. The 1.09 - 1.19 μm band does not match the ferric or ferrous iron absorption features at 0.95 and 1.0 μm respectively, and therefore cannot be justified on that basis.

The 1.55 - 1.75 μm region has also been shown in many studies to be a good band for vegetation classification. In this region the controlling factor in vegetation reflectance is the water content of the foliage. This band is thus a useful one for discriminating live

from dead vegetation. Its selection second for rock type discrimination is probably a consequence of the vegetation content of most of the rock type training sets.

Comments similar to that for the 1.55 - 1.75 μm band can be made for the 2.05 - 2.35 μm band. The conclusion of the spectral band analysis is that despite variations in data quality from band to band, optimum channels selected are well matched to major vegetation and rock type spectral reflectance features. Bands in the yellow, red, and near infrared were most useful. These bands represent narrowed, and slightly better placed bands than ERTS bands, plus two bands in the 1.5 - 2.5 μm region which ERTS did not have. The latter two bands have been consistently recommended as good bands in EOS Thematic Mapper studies.

3.3.2 FINAL MAP CATEGORIES, COMPARED WITH ERTS

After consultation between Mr. Ranson and ERIM personnel, a final set of classes to be displayed were selected. These classes are shown in Table 16 along with the classes mapped from the ERTS data collected on 20 August 1972 and reported in reference 10. Because of a misunderstanding between Mr. Ranson and ERIM, the Niobrara Shale signature was omitted from the final recognition map shown in Figure 26. There had been preliminary indications that the Niobrara Shale could be reliably discriminated from other rock types using the S-192 data.

Analysis of Table 16 reveals that the subjective analysis of recognition accuracy in test sites and the objective analysis of pairwise probabilities of misclassification from the channel selection program STEPL convinced Mr. Ranson that the sedimentary rock types, with the exception of Niobrara Shale, could not be accurately separated by the S-192 data. A quantative analysis of accuracy of recognition to be performed by Dr. Smedes and Mr. Ranson will reveal the accuracy of mapping the composite sedimentary rock class.

Further, the intermediate forest class, consisting of intermediate cover coniferous forest over various rock type substrates, was not formed

TABLE 16

FINAL MAP CLASSES FOR ERTS AND S-192
COMPUTER MAPPING OF CRIPPLE CREEK TEST SITE

ERTS	S-192
Niobrara Shale	(Niobrara Shale)
Pierre Shale	
Limestone	Undivided Sedimentary Rocks
Dakota Sandstone	
Fountain Formation	
Gruss	Pikes Peak Granite
Forest	Forest
Intermediate Forest	
Grassland	Undivided Volcanic - Plutonic Rocks
Meadow	Meadow
Water	Water
Cloud Shadow	Cloud Shadow
(Cloud and Snow)	Cloud and Snow

for the S-192 results. Instead these categories were lumped into either the undivided volcanic-plutonic rocks or the Pikes Peak granite classes, depending on the substrate. It was judged not possible to separate the various "exposed" volcanic-plutonic rocks with ERTS data, and these classes were lumped into a composite grassland category. Pikes Peak granite was judged separable from the other volcanic-plutonic rocks (granodiorite, phonolite, Cripple Creek granite, and volcanics) in the S-192 data.

The other categories were similar between the ERTS mapping and S-192 mapping efforts. The water category probably could have been separated from the cloud shadow category, but the same misunderstanding which caused the omission of the Niobrara Shale signature caused the omission of the water signature in the final classification results.

3.3.3 QUANTITATIVE CLASSIFICATION ACCURACY OF THE S-192 RECOGNITION MAP

Quantitative recognition accuracy of the map will be assessed by Dr. Smedes and Mr. Ranson. Because accuracy figures were not available at the time this report was written, we are unable to include these numbers.

3.4 CONCLUSIONS

Several conclusions were reached as part of this study of land cover mapping in the Colorado Mountain Area near Cripple Creek. First, six useful channels for discriminating vegetation and and rock classes were selected. These bands were narrowed versions of the four ERTS bands plus two bands in the near infrared region from 1.55 - 2.35 μm. Most of the bands selected can be justified on the basis of the reflectance spectra of vegetation and rock types. The lack of correlation of channel selection ordering with noise equivalent reflectance in each band is indicative that reflective band data quality did not play a major role in the selection of channels.

There was preliminary evidence that sedimentary rock type discrimination could be done more precisely with ERTS data than with S-192 data, perhaps because of the relatively higher noise equivalent reflectances of the S-192 channels. A final conclusion regarding this hypothesis must await quantitative accuracy evaluation of the S-192 recognition map to be performed by Dr. Smedes and Mr. Ranson.

In spite of a time of data collection near solar noon, the thermal channel was only the fifth most useful band for general classification (all scene categories) and seventh most useful for rock type classification. This result is at odds with studies made using aircraft data (e.g., reference 6) and may be explained by the relatively large 2.3° noise equivalent temperature of the thermal band on the SL-3 mission. To this extent then, the data quality of the thermal channel did influence the order of channel selection.

REFERENCES

1. R. E. Turner and M. M. Spencer, "Atmospheric Model for Correction of Spacecraft Data," in Proceedings of the Ninth Symposium on Remote Sensing of Environment, Environmental Research Institute of Michigan, Ann Arbor, October 1972.

2. L. Elterman, "Vertical Attenuation Model with Eight Surface Meteorological Ranges 2 to 13 kilometers," Report AFCRL-70-0200, Air Force Cambridge Research Laboratories, Office of Aerospace Research, Bedford, Massachusetts, 1970.

3. D. Zuk and G. Suits, "Report of Optical Ground Truth Measurements for 5 August 1973, Test Site Number 548532, in Support of the Skylab Multispectral Scanner," Report 101700-10-X, Environmental Research Institute of Michigan, Ann Arbor, Michigan, January 1974.

4. G. H. Suits, "The Calculation of the Directional Reflectance of a Vegetative Canopy," Remote Sensing of Environment, V. 2, pp. 117-125, 1972.

5. _____, "Sensor Performance Report Volume III (S-192) Engineering Baseline, SL-2, SL-3, and SL-4 Evaluation," Report MSC-05528, NASA, Johnson Space Center, Houston, Texas, September 1974.

6. F. J. Thomson, J. D. Erickson, R. F. Nalepka, and J. D. Weber, "Multispectral Scanner Data Applications Evaluation — Volume I — User Applications Study," NASA-JSC-09241, ERIM 102800-40-F, Environmental Research Institute of Michigan, Ann Arbor, Michigan, December 1974.

7. R. F. Nalepka, W. A. Malila, and J. P. Morgenstern, "Developing Processing Techniques for Skylab Data, Monthly Progress Report, May 1975," Report 101900-57-L, Environmental Research Institute of Michigan, Ann Arbor, Michigan, June 1975.

8. W. A. Malila, R. H. Hieber, D. P. Rice, J. E. Sarno, "Wheat Classification Exercise, Using 11 June 1973 ERTS-MSS Data for Fayette County, Illinois," Report 109100-21-R, Environmental Research Institute of Michigan, Ann Arbor, Michigan, September 1973.

9. _____, "Corn Blight Watch Experiment Final Report - Volume III," available from NASA, Johnson Space Center, Houston, Texas.

10. F. Thomson and F. Sadowski, "A Study of Atmospheric Effects on Pattern Recognition Devices," Report 193300-62-F, Environmental Research Institute of Michigan, Ann Arbor, Michigan, July 1975.

11. M. Gordon and J. Erickson, "Multispectral Scanner Data Processing Algorithm Documentation," Report 31650-149-T, Environmental Research Institute of Michigan, Ann Arbor, Michigan, July 1973.

12. F. J. Kriegler, "MIDAS Prototype Multivariate Interactive Digital Analysis System — Phase I," Volume I - System Description, Report 195800-25-F, Environmental Research Institute of Michigan, Ann Arbor, Michigan, August 1974.